6

Continental Fault Structure and Rheology from the Frictional-to-Viscous Transition Downward

MARK R. HANDY[1], GREG HIRTH[2], and ROLAND BÜRGMANN[3]

[1]Department of Earth Sciences, Freie Universität Berlin, Malteserstr. 74–100, 12249 Berlin, Germany
[2]Department of Geology and Geophysics, Woods Hole Oceanographic Institution, MS#8, WH01, Woods Hole, MA 02543, U.S.A.
[3]Department of Earth and Planetary Science, University of California, Berkeley, 389 McCone Hall, Berkeley, CA 94720, U.S.A.

ABSTRACT

Faulting is an expression of the interaction between rock rheology, kinematic boundary conditions, and associated stress fields. The structure and rheology of faults vary with depth, such that pressure-dependent frictional behavior predominating in the upper, brittle part of the crust is transitional to strongly temperature- and rate-dependent behavior in the lower part of the crust and mantle. This frictional-to-viscous transition (FVT) is characterized by changes in rock structure, rheology, and fluid activity that are closely tied to the earthquake cycle. As such, the FVT is a first-order decoupling zone, whose depth and lateral extent vary in time. Brittle, sometimes seismic, instabilities perturb the ambient stress field within the lithosphere on timescales ranging from seconds to years. These instabilities are measurable as transient motions of the Earth's surface and are manifest both at, and below, the FVT by the development of structural anisotropies (fractures, foliations). Surface motion studies of plate-boundary strike-slip faults indicate that shearing below the FVT is more localized in the lower crust than in the upper mantle. Structural investigations of exhumed shear zones reveal that this localization involves the nucleation of fractures at the FVT, as well as the buckling and rotation of existing foliations below the FVT. In some cases, rotation of these surfaces can initiate transient deformation, transferring stress upward and potentially triggering earthquakes. The networking of shear zones on several length scales allows them to function as decoupling horizons that partition three-dimensional strain within the lithosphere. The simplification of fault geometry with progressive

strain lends justification to the use of laboratory-derived flow laws to estimate the bulk rock rheology on length scales at which strain is homogeneous. In general, the longer the time- and length scales of faulting considered, the greater the potential influence of the kinematic and thermal history on the rheology of the fault system. Taken together, studies suggest that future fault modeling must include parameters that quantify the thermal and structural aspects of rock history, as well as the fluid activity in and around faults.

INTRODUCTION

This chapter addresses processes controlling the structure and rheology of fault zones in the lithosphere, from the frictional-to-viscous transition (FVT) down-wards. We define the FVT as the change from fracture and frictional sliding on one or more discrete surfaces to thermally activated creep within zones of vis-cous, solid-state flow. Such zones of continuous, distributed flow are variously referred to as shear zones, ductile shear zones, or ductile faults. Cataclastic fault rocks predominate above the FVT, whereas mylonitic rocks form at the FVT and below (e.g., Schmid and Handy 1991). In accordance with conven-tion, we use "fault" for any brittle shear surface and "shear zone" for a zone of viscous, predominantly mylonitic creep, irrespective of the ductility (i.e., distributedness) of the deformation on a given length scale.

    In the familiar lithospheric strength model, the FVT occupies a depth interval in the lithosphere between brittle deformation at the surface and predominantly viscous flow at greater depths in the crust and mantle. The FVT is usually depicted to coincide with a strength maximum between the brittle upper crust and the vis-cously deforming layers of the lower crust and mantle (Brace and Kohlstedt 1980). Such rheological stratification provides a first-order explanation of the architec-ture of orogens and passive continental margins on timescales of 10–100 Ma (e.g., Ranalli and Murphy 1987). However, as illustrated for an idealized strike-slip fault in Figure 6.1, this model needs to be modified to explain a variety of fault-related processes active on a much broader range of time- and length scales. The cyclical nature of seismicity provides a convenient measure of time for our discus-sion of fault evolution: Long, interseismic periods of near steady-state motion alternate with short periods of transient motion (coseismic, postseismic periods in Figure 6.1). We emphasize, however, that the FVT does not necessarily coincide with the transition from seismic to aseismic slip in the crust, which can represent a strain- and time-dependent change from unstable, stick-slip motion to stable frictional sliding on fault surfaces above the FVT (see Chapter 5).

    This paper is structured around a series of questions addressing some basic issues in fault dynamics. In raising these questions, we highlight some of the discrepancies between nature, experiment, and theory regarding the behavior of Earth's lithosphere and upper mantle. Our goal in this paper is to show how current thinking and state-of-the-art approaches may be applied over a range of scales to yield better insight into fault dynamics at, and below, the FVT.
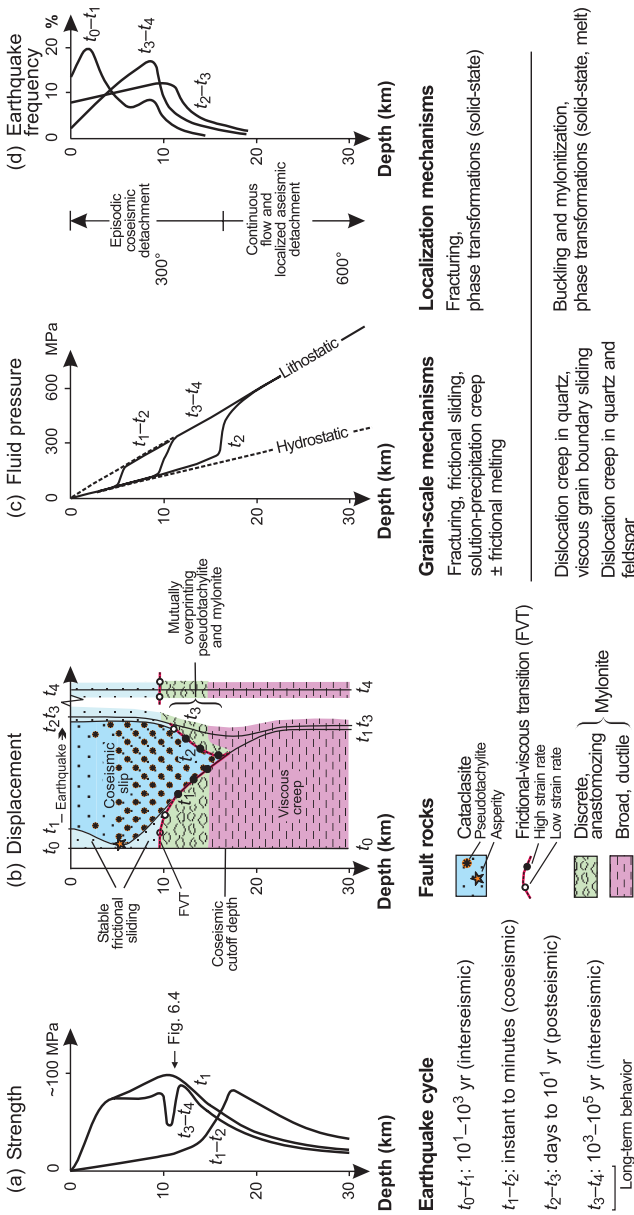
Figure 6.1 Characteristics and processes of an idealized strike-slip fault in continental crust during one earthquake cycle. (a) Strength *vs.* depth: arrow indicates depth for deformation mechanism map in Figure 6.4. (b) Displacement *vs.* depth: each line represents the locus of points along the fault surface at a given time (one line each for times t_0 to t_4), but the time interval between any two neighboring lines is not identical (modified from Tse and Rice 1986). Star marks fault nucleation on an asperity. (c) Pore-fluid pressure *vs.* depth. (d) Earthquake frequency (in % of earthquakes) *vs.* depth. Figure modified from Handy and Brun (2004). Maximum strength estimate in (a) taken from Handy et al. (1999). Earthquake frequency curves in (d) adapted from Rolandone et al. (2004).

RESEARCH TRENDS AND PROBLEMS

What Goes On at the Frictional-to-Viscous Transition?

Most knowledge of the FVT derives from experiments and microstructural studies of naturally deformed rocks. The view of the FVT as the site of a lithospheric strength maximum is based on the extrapolation of laboratory-derived constitutive equations for steady-state frictional sliding and power-law creep to natural strain rates and temperatures. The result is a strength-depth envelope similar in form to curve t_1 in Figure 6.1a. Taken at face value, some observations are consistent with this simple model. For example, stress measurements near the surface show an increase in stress with depth (Zoback and Townend 2001), and earthquake frequency and coseismic stress drop often peak within the same depth interval as the purported strength maximum (Meissner and Strehlau 1982; Scholz 1998). Also, stress-dependent microstructures in exhumed mylonitic fault rocks from near the FVT indicate higher differential stresses (~100 MPa, Stipp et al. 2002) than in originally warmer, hydrous crustal rocks from deeper crustal levels (e.g., 1 to tens of MPa, Etheridge and Wilkie 1981, see below).

When assessing this simple model, it is important to be aware of the assumptions upon which it rests, as well as of some frequently held misconceptions. Implicit in the construction of strength-depth envelopes is the view that rheology is solely a function of temperature, effective pressure and strain rate, and in some cases, grain size. Other simplifying assumptions include a steady-state geotherm, a uniform strain rate (or stress), and rock strength that is independent of length scale. In most tectonic settings none of these assumptions are likely to be strictly correct, as discussed in Handy and Brun (2004). Furthermore, strength-depth envelopes are commonly calculated for a single deformation mechanism in the viscous deformational regime (most often dislocation creep). Microstructural studies of fault rocks, however, indicate that deformation mechanisms at the FVT evolve with strain, and that several grain-scale deformation mechanisms with different temperature, pressure, and strain-rate dependencies accommodate the bulk strain and strain rate, as shown in Figures 6.2 and 6.3, and discussed below. Competing deformation mechanisms at the FVT are also observed in experiments, for example, on granite (Dell Angelo and Tullis 1996), quartzite (Hirth and Tullis 1994), marble (Fredrich et al. 1989), halite (Chester 1988), and mica-quartz aggregates (Bos et al. 2000; Bos and Spiers 2002). Finally, there has been a tendency in the literature to relate seismicity to rock strength (e.g., Jackson 2002) despite the fact that seismicity is at best an ambiguous indicator of strength (Handy and Brun 2004). The realization that frictional properties and permeability within fault zones are time dependent has led to the notion of the FVT as a depth interval marked by significant fluctuations in strength (Scholz 1998) and fluid pressure (Sibson and Rowland 2003), especially on short time- and length scales. These fluctuations are closely tied to the earthquake cycle, as depicted schematically in Figure 6.1c.
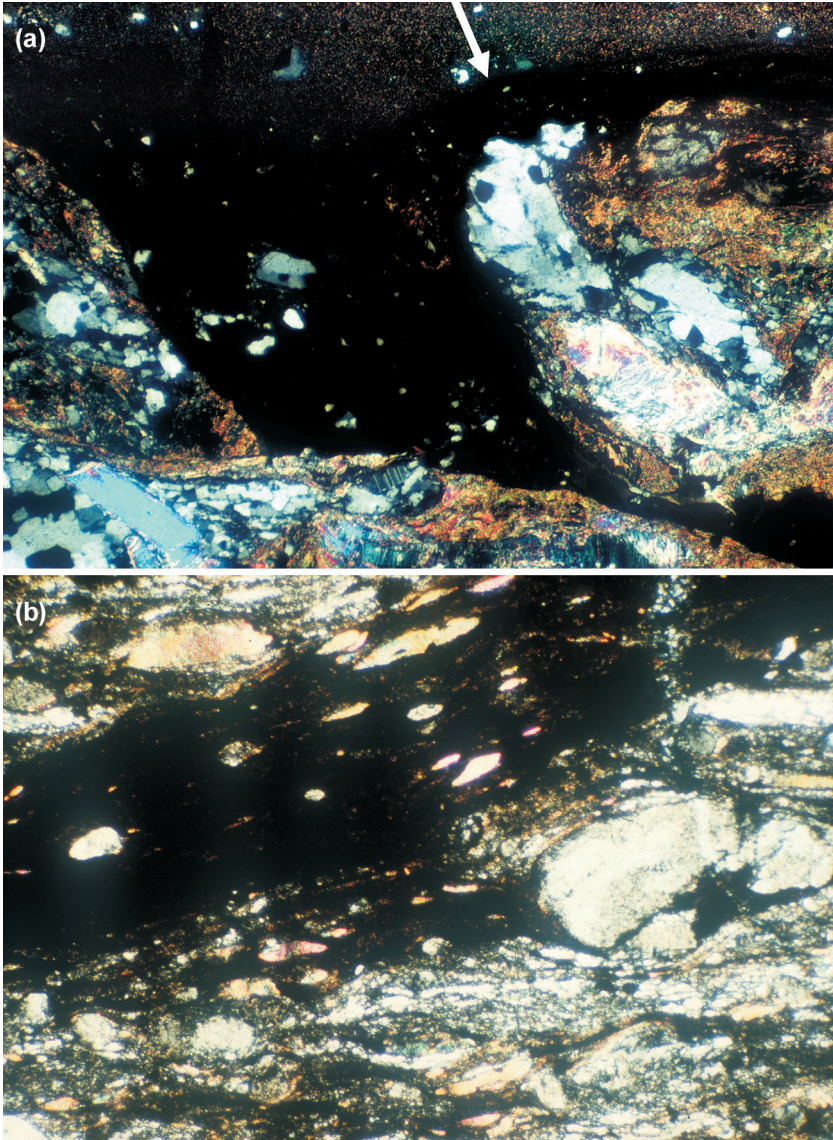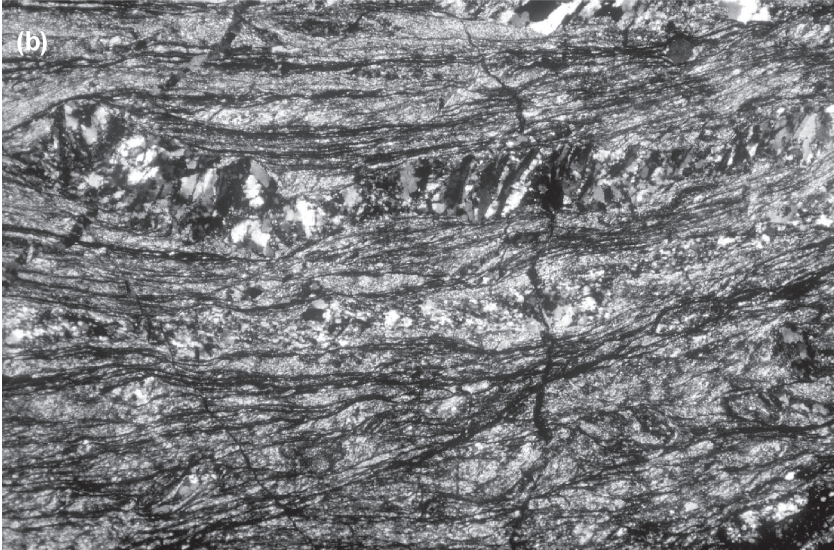
Figure 6.2 Microstructures of the coseismic frictional-to-viscous transition (FVT) in which a pseudotachylite vein cuts a mylonite in (a) and is itself overprinted in (b) by mylonite during postseismic to interseismic mylonitic creep. The arrow in (a) points to the boundary between glassy chilled margin and aphanitic, devitrified vein interior. The protolith of the black ultramylonite in (b) is the pseudotachylite vein in (a). Note the rounded clasts of mica in (b) indicative of mylonitic overprinting. Crossed polarizers, dimensions 2.0 × 1.3 mm). Samples taken from the Pogallo ductile fault zone, southern Alps, northern Italy (Handy 1998).

Interseismic strain leads to the buildup of stress, with differential stress at the FVT approaching a maximum (t_0 to t_1; Figures 6.1a, 6.1b). This stress is released suddenly along a rupture surface that nucleates at an irregularity in the fault surface (marked with a star in Figure 6.1b). This irregularity can be an asperity, that is, a rough or uneven part of the fault, a pocket of anomalous pore-fluid pressure, or a change of mineralogy along the fault surface. The effect of the irregularity is to allow local stress levels to attain the fracture (or frictional) strength of the rock or to reduce fracture strength to the local stress level. Either case favors failure and rapid localization of strain.

During coseismic faulting, fractures propagate down into crust (curves t_1 to t_2; Figure 6.1b), which deforms viscously during interseismic periods. Figure 6.2 shows a natural example of this: mylonite is cut by pseudotachylite (Figure 6.2a), which is itself subsequently deformed by mylonite (Figure 6.2b). The depth and duration of this downward penetration depend on the area and amount of coseismic slip, reflected in the magnitude of the main earthquake event. For example, the $M_w = 7.3$ 1992 Landers earthquake along the San Andreas fault system in the southwestern United States led to a ~3 km depression of the base of the seismogenic zone (Figure 6.1d), which gradually decayed over a time of four to five years (Rolandone et al. 2004; see also Figure 2.11 in Chapter 2). The much smaller, $M_w = 6.2$ Morgan Hill earthquake resulted in only a ~500 m depression that recovered within two years (Schaff et al. 2002). Coseismic stress drops as great as 100 MPa (Bouchon 1997) have been recorded locally, but earthquake seismology indicates that the stress drop is usually one to two orders of magnitude less than this value and is unrelated to the magnitude of the main earthquake event (e.g., Kanamori and Heaton 2000). Indeed, the possibility that complete stress drops occur during earthquakes remains a controversial interpretation of the static stress drop observed during earthquakes (e.g., Scholz 1992). Geologic evidence for a coseismic transition

---

Figure 6.3 Microstructures of the aseismic frictional-to-viscous transition (FVT): (a) Veins ▶ with fibrous quartz-cut fine-grained mylonitic matrix comprising syntectonically recrystallized chlorite, white mica, and quartz. Note that the older, less-deformed vein at top right is at a higher angle to foliation than more deformed vein at bottom (crossed polarizers, dimensions 22.6 × 15 mm). (b) Rotated quartz veins with various degrees of mylonitic overprint are stretched parallel to the mylonitic foliation (crossed polarizers, dimensions 5.6 × 3.8 mm). The inference of coeval fracturing, fluid flow, and mylonitic creep in this sample comes from the mutual overprinting of veins and mylonitic foliation: Veins cut the foliation but are themselves increasingly deformed with decreasing angle to the mylonitic foliation The inferred deformation mechanisms are dislocation creep and viscous granular flow including pressure solution in the fine-grained matrix, fracturing, veining, and precipitation of quartz in the presence of a fluid phase in the fibrous quartz veins, and dislocation creep (subgrain rotation and grain-boundary migration recrystallization of quartz fibers) in the veins. Sample was taken from the same shear zone as in Figure 6.2.

from viscous to brittle deformation comes from mutually overprinting pseudot-
achylite and mylonite (e.g., Hobbs et al. 1986 and Figure 6.2) and from micro-
structures in quartz-rich crustal rocks indicative of transient differential stresses
much higher than average flow stresses in the viscous crust (= 300–500 MPa,
Küster and Stöckhert 1999). Küster and Stöckhert (1999) and Trepmann and
Stöckhert (2003) interpret these microstructures to have formed during coseismic
elastic loading followed by rapid postseismic relaxation in the vicinity of a
rupture surface, although no traces of such a surface leading down from a fossil
FVT have been found so far in their example.

Postseismic deformation is highly transient, with the magnitude of change
in the strain rate of the viscous crust determined by the amount of coseismic
slip in the brittle, upper crust (t_2 to t_3 in Figure 6.1b). During reinitiation of
long interseismic periods (t_3 to t_4 in Figure 6.1) the FVT is inferred to be a site
of localized shearing and therefore to have reduced strength relative to the ad-
jacent over- and underlying rocks. This hypothesis is supported by the preva-
lence at the FVT of very fine grained (1–10 μm), mylonitic fault rocks with
microstructures diagnostic of viscous granular flow as well as by the presence
of recrystallized hydrous minerals that are intrinsically weak (e.g., biotite, white
mica). Figure 6.3 shows an example of the aseismic FVT, where dislocation
creep, viscous granular flow, fluid-assisted veining, and precipitation of quartz
are inferred to have occurred simultaneously. Abundant geologic evidence in-
dicates that anastomozing shear zones at the FVT act as detachment surfaces
within the crust (Handy and Brun 2004).

To illustrate the possible effects of stress- and strain-rate fluctuations during
faulting, we show a deformation mechanism map in Figure 6.4 for quartz-rich
rocks at conditions for the FVT in Figure 6.1. Three of the mechanisms identi-
fied in the example above are represented in Figure 6.4 (cataclasis, dislocation
creep, viscous granular flow), although explicit constitutive formulations are
not possible for all of them due to the limited rheological data (sources in the
caption). In particular, the field for pressure-solution creep must be regarded as
broadly representative of several different types of viscous granular flow in-
volving fluid-assisted, intergranular diffusion (e.g., Paterson 1995). Neverthe-
less, experiments allow us to place the following general constraints on rock
strength (e.g., Kohlstedt et al. 1995), as depicted in Figure 6.4: First, the transi-
tion from localized (faulting) to distributed (ductile) deformation ("semi-brittle
flow" in experimentalist's parlance) occurs when rock strength becomes less
than that required for stable frictional sliding. A reasonable upper bound for
this stress is obtained from Byerlee's (1978) empirical relation, often referred
to as "Byerlee's law," modified for effective stress at hydrostatic pore-fluid
pressure, as shown in Figure 6.4. This frictional stress is an upper bound to
rock strength because pore-fluid pressure can exceed hydrostatic values and
because some fault zone materials have very low frictional coefficients that do
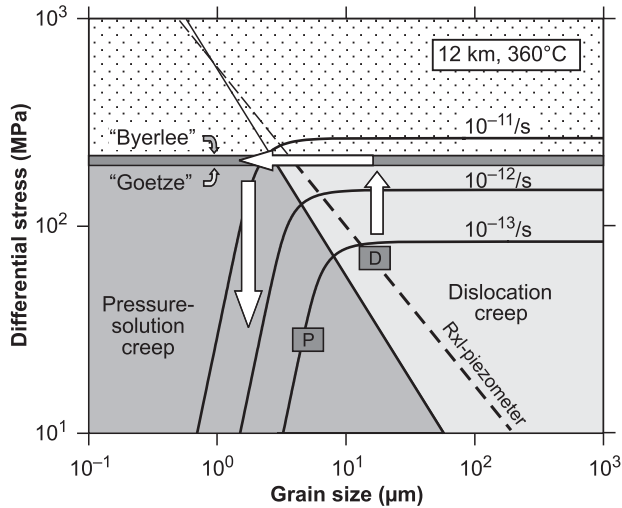not obey Byerlee's law (e.g., some clays [Byerlee 1978], serpentine [Moore

Figure 6.4 Deformation mechanism map for quartz-rich rock at the FVT at 12 km and 360°C, corresponding to the depth indicated with the arrow in Figure 6.1a. Strain-rate contours in the dislocation creep field are from Hirth et al. (2001), in the viscous granular flow field from Kenis et al. (2005) for pressure-solution creep. The thick line separates these mechanism fields, whereas the dashed line labeled "rxl-piezometer" is the quartz recrystallized grain-size piezometer of Stipp and Tullis (2003). Thin continuation of all these lines in the stippled area is only valid for creep at pore-fluid pressures less than hydrostatic. Boxes labeled P and D indicate deformational conditions, respectively, for fine-grained siliciclastic rocks undergoing pressure-solution creep (Kenis et al. 2005; Schwarz and Stöckhert 1996) and for coarser-grained quartzite undergoing dislocation creep (Dunlap et al. 1997). The line labeled "Byerlee" shows frictional stress for a strike-slip fault along a hydrostatic pore-fluid pressure gradient. Stresses in the stippled field above this line exceed the fracture strength and hence are not realizable at hydrostatic pore-fluid pressure. The line labeled "Goetze" represents conditions at which differential stress equals the least principal stress. White arrows illustrate a possible stress–grain-size path during and just after an earthquake, corresponding to intervals t_1–t_2 and t_2–t_3 in Figure 6.1a. See text for explanation. Fluid-assisted veining is not shown explicitly in Figure 6.4 but occupies the stippled field above the horizontal line representing Goetze's criterion. An increase of pore-fluid pressure above hydrostatic values would shift this line downward, consistent with embrittlement at lower differential stresses.

et al. 1997]). Both conditions would shift the horizontal line in Figure 6.4 marked "Byerlee" to lower values of differential stress. Second, viscous creep is expected when rock strength ($\Delta\sigma = \sigma_1 - \sigma_3$) becomes less than the least principal stress (σ_3), an empirical relation referred to as "Goetze's criterion." For the stress state on strike-slip faults outlined by Zoback and Townend (2001), Goetze's criterion is satisfied when $\Delta\sigma = (2\rho gh)/3$, where ρ is rock density, g is the acceleration of gravity, and h is depth or height of the rock column. As illustrated in

Figure 6.4, this differential stress is similar to that predicted for frictional sliding by Byerlee's law at hydrostatic pore-fluid pressure, lending credence to a strength maximum at the FVT, at least for some intervals of the interseismic period (near t_1 in Figure 6.1a).

During the long interseismic periods, rock strength from the FVT downward is limited by viscous granular flow in fine-grained micaceous rocks as well as by dislocation creep in relatively coarse-grained, quartz-rich rocks (boxes P and D in Figure 6.4). This is consistent with experimental data indicating that diffusion creep is not rate competitive in pure quartz aggregates at geologic conditions (Rutter and Brodie 2004). However, major changes in grain-scale mechanisms are expected to occur during co- and postseismic intervals, as shown by the white arrow in Figure 6.4. The increase of strain rate during coseismic rupture results in rapidly increased stress and therefore effects a transition from dislocation creep to cataclasis. Grain-size reduction and gouge formation due to cataclasis and fluid-enhanced mineral reactions promote a transition to viscous granular flow (Figure 6.4, e.g., Handy 1989) and an associated increase in strain rate. Depending on the extent of grain-size reduction, postseismic creep rates can be high while occurring at relatively low differential stresses. Creep rates may be further enhanced by increased porosity owing to dilation during rupture (Sleep 1995). The subsequent strength evolution depends on postseismic microstructural changes. Fault-sealing involving porosity reduction and cementation, or syntectonic grain growth (Gratier and Gueydan, see Chapter 12), can induce a return to dislocation creep with a related increase in strength. Alternatively, rock strength at the FVT may remain low, as shown in Figures 6.1a and 6.4, if newly crystallized minerals (e.g., phyllosilicates) pin grain boundaries; the average grain size remains small, promoting continued dominance of viscous granular flow. At greater depths below the FVT, the stress increase associated with an earthquake rupture above may not be sufficient to induce embrittlement. There, dislocation creep will be favored, even where long-term creep involves viscous granular flow.

In summary, the FVT is a zone marked by spatiotemporal variations in rock strength, mineralogy, and fluid activity that are related to the earthquake cycle, as illustrated in Figure 6.1. These fluctuations make the FVT a first-order mechanical discontinuity that often serves as a major decoupling horizon within the lithosphere.

The model shown in Figure 6.1 pertains to a strike-slip fault with no significant dip-slip motion. Large thrust faults in subduction zones and extensional faults in rifted margins may deviate from this behavior, especially due to changes in fluid availability in the vicinity of metamorphic reactions. For example, prograde reactions in rocks undergoing burial are associated with a decrease in volume and tend to release volatile phases, potentially leading to local embrittlement, and possibly even triggering seismicity, as proposed for intermediate-depth earthquakes along megathrusts in some subducting slabs (Hacker

et al. 2003). In such depth intervals, the transition from viscous creep to frictional behavior (and back) is ephemeral, strain dependent, and controlled by reaction kinetics and permeability evolution (Miller 2002; Miller et al. 2003). Conceivably, such faults have several short-lived FVTs beneath the primary, long-term FVT described above, with strength and pore-fluid pressure curves that evolve differently from those shown in Figure 6.1.

How Can the Fossil Frictional-to-Viscous Transition Be Identified in Nature?

Criteria for identifying the fossil FVT in naturally deformed rocks include the structural continuity of fractures, cataclasite and mylonite formed at identical metamorphic conditions, as well as mutually overprinting relationships between fractures, cataclasite and mylonite on a given length scale of observation (Figure 6.5, Handy 1998). These criteria can be used on the outcrop and regional scales, as well as on the grain scale (Figures 6.2, 6.3). Unfortunately, tracing exhumed tracts of a fossil FVT over areas of 10–100 km^2 is hampered by later fault reactivation and by the difficulty of distinguishing coexisting cataclastic and mylonitic fault rocks at the FVT from cataclastic overprinting that all mylonitic fault rocks experience during exhumation. Recognizing the FVT on such large length scales requires excellent exposure and considerable topographic relief.

Exhumed FVTs are best preserved along the tops of the footwalls of low-angle normal faults (the so-called metamorphic carapace) within metamorphic core complexes, as depicted in Figure 6.6. There, the preservation of FVT structures is
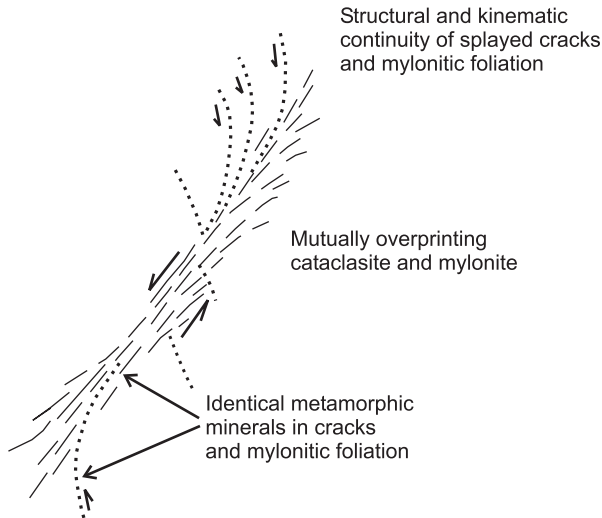

Figure 6.5 Diagnostic feature of the frictional-to-viscous transition (FVT) on the outcrop and map scales.
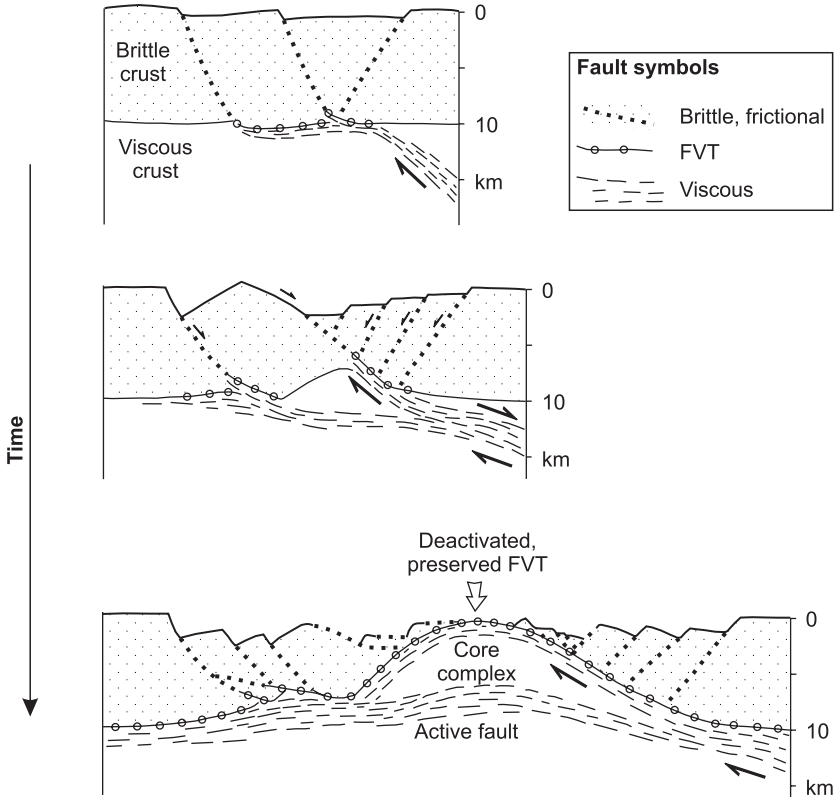
Figure 6.6 Progressive exhumation of the frictional-to-viscous transition (FVT) during crustal extension. Figure modified from Brun et al. (1994).

facilitated by strain localization during extensional denudation and cooling of the core, as shown in detail in Figure 6.7a (see also Handy 1986). The spatial distribution of microstructures within the fault reflects the fault orientation and rate of shearing with respect to the transient isothermal surfaces in the footwall of the fault. The extent of microstructural preservation depends on the rock's trajectory and, hence, on its thermomechanical history during exhumation (Figure 6.7b). Generally, preservation of the FVT in quartz-feldspar-mica rocks is best in a narrow domain of discrete, anastomosing mylonite (marked B in Figure 6.7) that experienced episodic embrittlement during exhumation through the 300–500°C range. The domains on either side of B either never experienced episodic embrittlement (C), or were affected by various degrees of brittle overprinting (A) or annealing (D). Progressive cooling and hardening of the top of the exhuming core complex can lead to a downward jump of deformation into weaker, partially melted layers (bottom of Figure 6.6). This deactivates faults along the crest of the arched core complex and so protects the FVT from brittle overprinting.
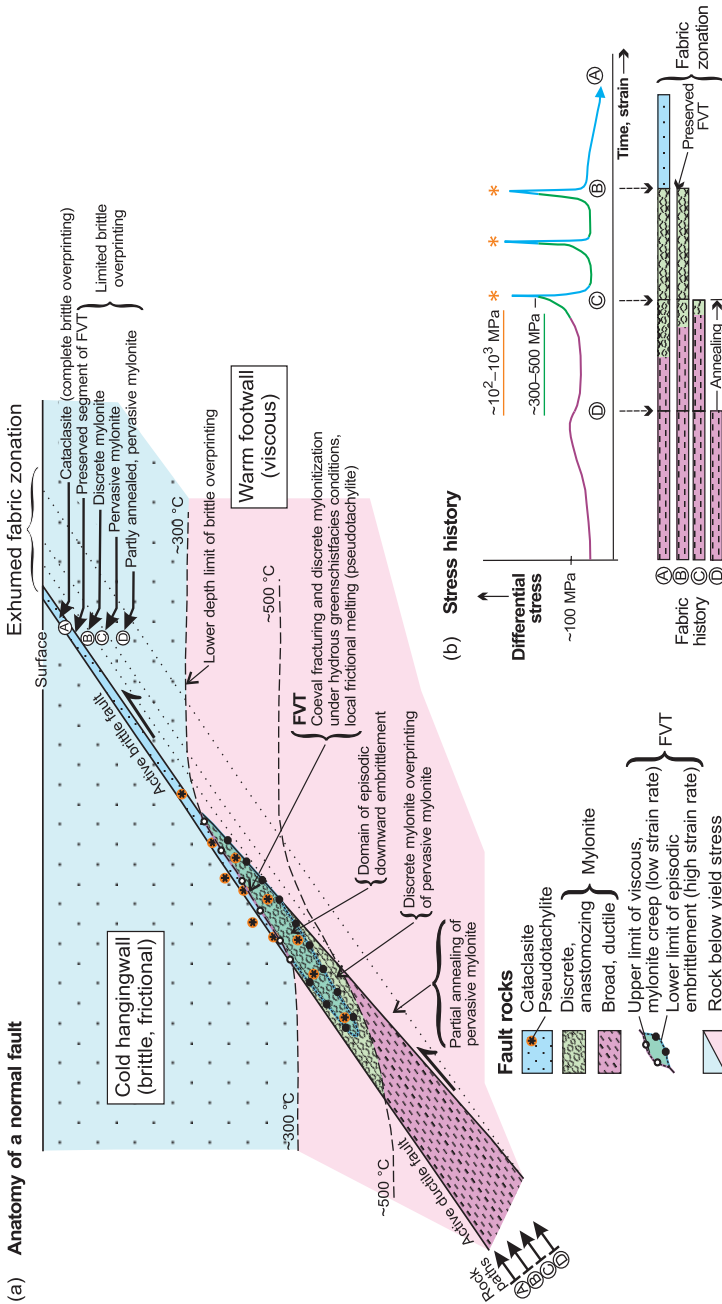
Figure 6.7 Generic cross section through a normal fault, based on an example in the Southern European Alps (Handy 1998): (a) zonation of fault rock fabrics, including the frictional-to-viscous transition (FVT), with respect to isotherms and the surface; (b) hypothetical stress and fabric histories for rock exhumation paths A–D in different parts of the fault in (a). Differential stress estimates in (b) taken from Etheridge and Wilkie (1981) and Otsuki et al. (2003).

Ancient thrust systems are less likely to preserve relics of the FVT due to overprinting during footwall collapse and/or subsequent folding, whereas faults with a large strike-slip component are steep, rendering exposure of the subhorizontal FVT fortuitous. Only where blocks of crust containing an older strike-slip fault have been rotated and/or differentially eroded, for example, in younger orogenic belts or on rift shoulders, can one expect to find continuous outcrops of the tilted and exhumed FVT.

Searches for fossil FVTs can be mounted using a combination of structural and thermochronological methods. The 270–350°C temperature range of the FVT in quartz-rich rocks (Dunlap et al. 1997; Handy et al. 1999; Stöckhert et al. 1999) coincides generally with the diffusional closure temperatures of the Rb-Sr biotite, Ar-Ar white mica, and biotite isotopic systems (Villa 1998) for a range of common grain sizes. Thus, mica cooling-age isochrons constructed from many analyses across metamorphic domes can delimit potential, temporal traces of the FVT in exhumed pelitic and granitic rocks. Once a fossil FVT is identified, dating it can be a challenge fraught with analytical and interpretational difficulties. For example, conventional Ar-Ar dating and *in situ* laser mapping of pre- and syntectonic white micas from a fossil FVT along an exhumed extensional fault yielded a range of post-tectonic Ar-Ar ages within compositionally homogeneous grains (Mulch et al. 2002); the variable ages turned out to reflect defect-enhanced diffusive argon loss controlled by intragranular microstructures formed during deformation. These microstructures reduced the effective grain size to less than the grain size observed in thin section (Mulch et al. 2002). In a different example, however, a close correlation of intragranular age and composition in different white mica microstructures formed during sequential crystallization faithfully documented progressive deformation (Mulch and Cosca 2004). Obtaining a reliable deformational age requires identifying the deformation mechanism(s) in the sample and understanding the effect of this mechanism on composition and grain size (Reddy and Potts 1999). Age versus grain-size relationships, microsampling (Müller et al. 2000), and *in situ* laser mapping of single grains all yield potentially valuable information on the relationship between measured isotopic ages and the time at which microstructures were formed and then effectively frozen. Constraining this relationship is crucial to determining the thermomechanics of the FVT.

How Do Mechanical Instabilities in the Viscous Lithosphere Nucleate and Grow?

Strain localization can be treated as a two-stage process involving the nucleation and growth of a mechanical instability, such as a shear zone. The inherent weakness of a shear zone relative to its surrounding, less-deformed, or undeformed wall rock drives localization. The deformational system is defined as the localizing shear zone plus its stable (or conditionally stable) surroundings.

Localizing instabilities can nucleate along material heterogeneities at scales ranging from individual grains to the lithosphere. In experiments, localization instabilities nucleate at material heterogeneities; these heterogeneities are either inherent to the experiment from the outset (e.g., the piston–sample interface) or must be introduced during the experiment (soft inclusions in an otherwise homogeneous medium). In fact, even in experiments designed for homogeneous deformation, it is sometimes difficult to avoid the nucleation of instabilities at the boundaries of the sample.

Continuum mechanical approaches have been developed to evaluate how strain localizes in the absence of an existing heterogeneity. Although such approaches may seem of little practical applicability to heterogeneous materials like rocks, they nevertheless bear some interesting implications for natural rock deformation. Continuum approaches to localization involve analysis of three separate criteria for the nucleation of a shearing instability (Hobbs et al. 1990): (a) stability, (b) bifurcation potential, and (c) bifurcation mode. A system becomes unstable if a small perturbation in its deformation amplifies, such that the strain energy or work performed decreases in the next increment of strain. A system can bifurcate if the deformational response to an applied stress is non-unique, that is, if deviation from a homogeneous, incremental strain field becomes possible. The bifurcation mode specifies the path of this deviation, that is, the manner and degree of strain localization. Important from the standpoint of rock deformation is that any deformation which involves a non-unique relationship between stress state and strain rate may become heterogeneous, usually while weakening, and in the case of dilatant materials, even while hardening (e.g., Rudnicki and Rice 1975). In viscous materials, the nucleation of an instability coincides with weakening of the deforming rock. For composite materials with a tendency to dilate (e.g., mylonitic rock with fractures or brittle inclusions), weakening may only initiate after the instability has grown to the point where it forms a through-going network subparallel to the shearing plane (Handy 1994a).

At conditions near the FVT, structural evolution associated with brittle and viscous mechanisms may lead to localization and concomitant weakening. For example, as described above, cataclasis may result in a reduction of grain size that is sufficient to promote viscous granular flow. Grain-scale weakening mechanisms that could promote localization without significant dilation include dynamic recrystallization by grain-boundary migration, texture development (crystallographic preferred orientation), and shear heating. Of these, only shear heating has yet to be unequivocally identified in shear zones. Perhaps this is because the adiabatic condition required for runaway thermal weakening only applies at anomalously high strain rates just below the FVT (Hobbs et al. 1986) where its traces are masked by postseismic and interseismic creep.

The role of syntectonic metamorphic reactions in localizing strain has been documented in nature and experiments for some time (e.g., Brodie and Rutter 1985, 1987), it but has been widely overlooked in modeling studies of

lithosphere-scale faulting and orogenesis. The nucleation of fine-grained products can weaken a rock drastically, especially if the reactants are deformed outside of their *P-T* stability field (thereby enhancing reaction rates) and if the reaction is exothermic (preventing it from freezing; Green and Burnley 1990; Kirby et al. 1991). The stress drop in the shear zone is larger for reactions with a large change in molar volume, which together with the exothermic condition, limits this type of seismic instability to prograde reactions at great depth in the upper mantle, for example, in subducting lithospheric slabs (e.g., Karato et al. 2001). Endothermic reactions, especially those involving a fluid phase, can also induce rapid weakening during initial fracturing and phase nucleation (e.g., eclogite-facies pseudotachylite and shear zones in granulites; Klaper 1990; Austrheim and Boundy 1994), but beyond this, grain growth tends to stabilize creep.

At a larger scale, buckling, or active folding of existing anisotropies, is a ubiquitous strain localization mechanism in the viscous lithosphere. Metamorphic rocks generally have one or more mechanical anisotropies (compositional banding, sedimentary layering, schistosity) that develop buckling instabilities, even if they are oriented obliquely to the greatest incremental shortening axis. In strain fields near simple shear, progressive rotation of the dominant anisotropy towards the macroscopic shearing plane—whether achieved by active or passive folding—is accompanied by a reduction in bulk rock strength as stress within the layers becomes increasingly uniform. Termed rotational weakening (Cobbold 1977), this process eventually leads to pervasive mylonitic shearing as the folds become isoclinal and the dominant anisotropy is transposed into the shearing plane. As discussed below, mechanical anisotropies on all scales tend to acquire stable orientations that are related to the kinematic framework.

Networking of shear zones is another growth mechanism that weakens rock over a wide range of scales. Individual shear zone strands rotate and coalesce to form interconnected, anastomozing weak layers that envelop and boudinage lozenges of less-deformed or undeformed wall rock. The proportion of weak shear zone to stronger lozenge rock increases until the entire deformational system approaches steady-state creep at a lower bulk strength than in its initial, unnetworked state (Handy 1994b).

Can Strain Localization below the Frictional-to-Viscous Transition Induce Transience? Can It Trigger Earthquakes?

Whereas progressive folding can lead to strain homogenization and weakening as outlined above, mylonitic shearing can remain heterogeneous to high shear strains. Evidence for this persistent heterogeneity comes from the prevalence of S, C, and C' shear surfaces at very high shear strains ($\gamma > 10$) in mylonitic fault rocks (Berthé et al. 1979; Platt and Vissers 1980). The example shown in Figure 6.8 comes from a retrograde, greenschist-facies, crustal-scale shear zone formed just below the FVT transition (Palm 1999). The shear bands (C' surfaces)
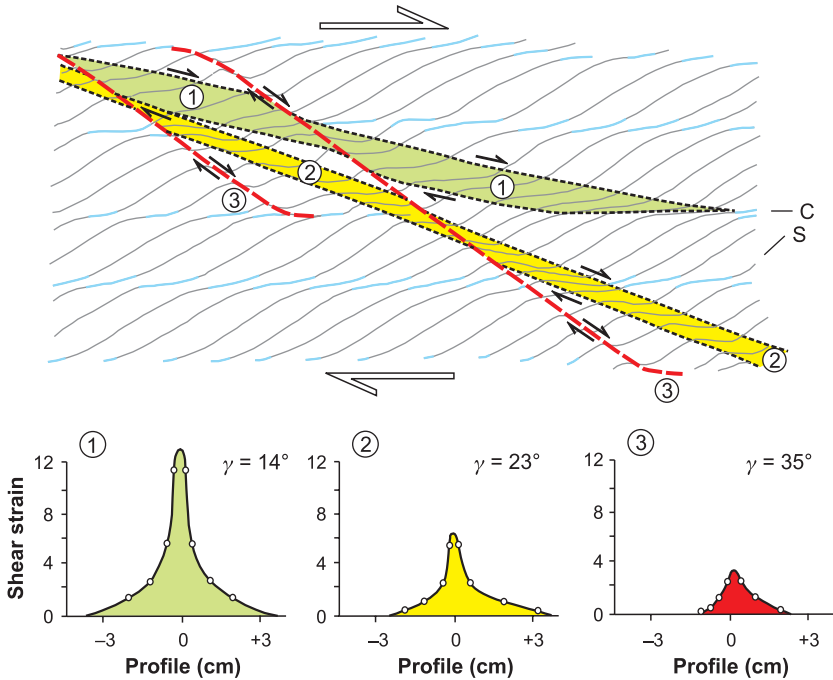
Figure 6.8 Coeval strain localization in newly nucleated shear bands, and broadening and lengthening of older, rotating shear bands in a retrograde, greenschist-facies mylonite (modified from Palm 1999). (a) Sketch of three sets of C' surfaces (shear bands), labeled 1–3 in order of decreasing age based on cross-cutting relationships. The shear bands are inferred to rotate anticlockwise, that is, antithetically, with respect to the overall dextral shear vorticity. (b) Shear strain calculated as a function of distance along profiles normal to the shear bands numbered in (a) using the foliation-deflection method of Ramsay and Graham (1970).

nucleated either as shear fractures or, more often, as hybrid, extensional shear fractures at moderate angles (20–35°) to the shearing plane (Figure 12 in Bauer et al. 2000). They then broadened, lengthened, and rotated antithetically (shear band 1, Figure 6.8) before being cut and displaced by successively younger C' surfaces (shear bands 2 and 3, Figure 6.8). The antithetical rotation of the shear bands reflects shortening normal to the shearing plane (C surfaces) during general (dextral) noncoaxial deformation, as predicted by the kinematic model of Platt (1984). Shear strain on the shear bands increased as they rotated away from their initial orientation and toward concordance with the macroscopic shearing plane, represented by the C surfaces (Figure 6.8).

The coeval nucleation and rotation of broadening shear bands are interpreted to have caused transient mechanical behavior on the length scale of these heterogeneities. The orientations of these shear surfaces, depicted in Figure 6.9a,
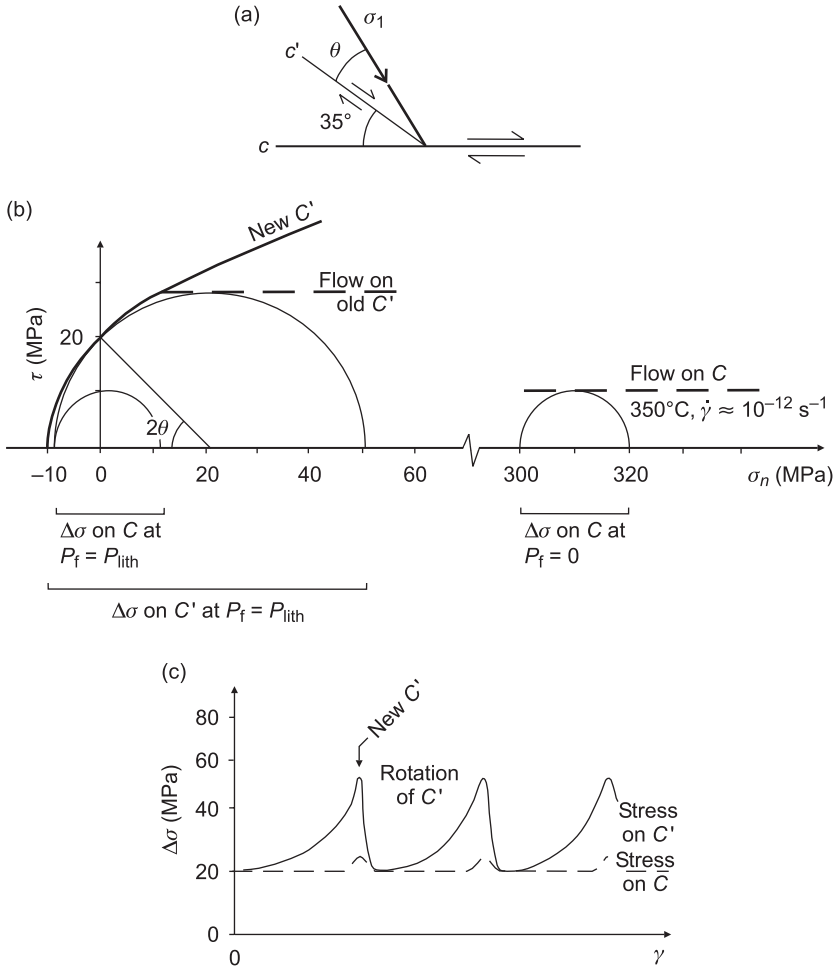
Figure 6.9 Geometry and stress states on shear surfaces for the rock in Figure 6.8. (a) Schematic representation of C and C' shear surfaces at the moment of formation of C' fractures. (b) Mohr diagram showing stress states used to constrain the stress drop at the moment of fracturing along the C' direction, as discussed in the text. (c) Episodic fluctuations of stress resulting from episodic shear band formation during continuous shearing.

form the basis for a first-order estimate of the local stress drop associated with the formation of a shear band. This estimate is obtained by subtracting the ambient, mylonitic flow stress on the S and C surfaces (6–34 MPa derived from paleopiezometry in dynamically recrystallized quartz grains in the same example above, Handy 1986) from the differential stress during hybrid fracturing across the S and C foliations ($4\sigma_T < \Delta\sigma < 2\sigma_T\sqrt{8}$, where σ_T is the

tensile strength of the unfractured rock, Secor 1965). Taking average values of 20 MPa for the mylonitic flow stress, 10 MPa for σ_T (Etheridge 1983) and an average fracture angle, Θ, of 22.5° for hybrid and shear fractures in the vicinity of the natural example above (Figure 6.9a), we obtain a stress drop of ~36 MPa at the moment of fracturing on C' (Figure 6.9). Stress drops of up to ~100 MPa are possible for higher values of σ_T (20 MPa, Etheridge 1983), lower values of ambient flow stress and/or for shear bands that initiate as shear fractures (30° > Θ > 22.5°) at the confining pressure of fault activity (~300 MPa; Handy 1986). Regardless of the magnitude of stress drop, antithetic rotation of the shear bands away from their initial, favorable orientation leads to progressive hardening until the differential stress locally exceeds the fracture strength of the rock and the next generation of shear bands develops (Figure 6.9c).

The example above serves to illustrate two points. First, new anisotropies nucleate in strongly anisotropic rocks when the existing anisotropies (e.g., S and C' surfaces in Figure 6.8) either become unfavorably oriented for creep and harden, or are insufficient in number to accommodate strain compatibly. Von Mise's criterion of ductility predicts that at least three independent slip systems are required for compatible plane strain deformation, and this minimum number of slip systems increases to five for general, three-dimensional deformation. Second, stress drops associated with the cyclical formation and rotation of new anisotropies are episodic on the length scale of the existing anisotropy (Figure 6.9c). However, are strength drops on the order of tens to a hundred MPa sufficiently large to trigger large-magnitude earthquakes?

The answer to this question is, conceivably, yes—provided that the shear surfaces develop quickly and on a sufficiently large length scale. As pointed out in the following section, C' surfaces in exhumed mountain belts exist on scales of one to tens of kilometers, possibly even hundreds of kilometers. A mechanism by which instabilities below the FVT might trigger seismic slip in the upper crustal part of a strike-slip fault is shown qualitatively in Figure 6.10. This diagram is modified from Figure 6.1b to illustrate the effect of weakening during a single episode of shear band formation on the crustal scale. From times t_{1a} to t_{1b}, weakening enhances the displacement rate below the FVT, thereby transferring horizontal displacement and stress upward into the brittle crust until the rock strength at the asperity (star in Figure 6.10) is exceeded at time t_{1b}. Vertical stress transfer, therefore, can trigger seismic instabilities in the upper crust earlier than if no shear bands had developed and displacement and stress had accrued continuously during homogeneous flow. Obviously, this mechanism is most effective when near-lithostatic pore fluid at the top of the viscous crust reduces the effective stress on potential fault surfaces. The feasibility of this mechanism awaits testing with appropriate mechanical models.
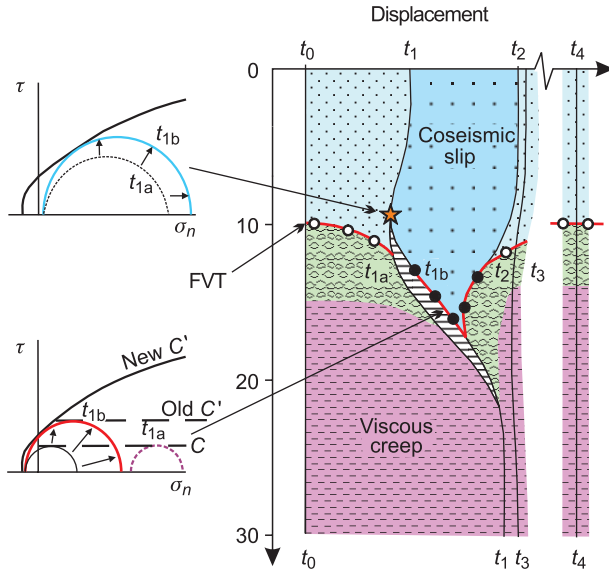
Figure 6.10 Displacement versus depth diagram as in Figure 6.1b, but illustrating accelerated displacement during a single episode of shear band development below the FVT from times t_{1a} to t_{1b} (vertically hatched domain). Vertical stress transfer during this time potentially triggers coseismic slip at an asperity (star) in the upper, brittle crust at time t_{1b} (see text for explanation). Mohr diagrams contain semicircles representing stress states at times t_{1a} (dashed semicircles) and t_{1b} (solid semicircles).

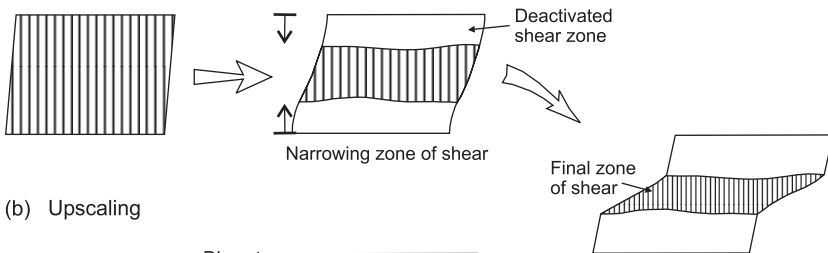## What Factors Affect the Geometrical Scaling Properties of Shear Zones?

Natural deformation is heterogeneous on some scales but homogeneous on others. Our goal is to understand under which conditions the assumption of homogeneous deformation is reasonable and how bulk rheology changes when strain becomes heterogeneous.

   The scales at which strain becomes localized are often controlled by existing mechanical heterogeneities in the crust and/or mantle. For example, centimeter-scale mylonitic shear bands scale with harmonics of the characteristic spacing between feldspar clasts in the protolith (Dutruge et al. 1995). In contrast, the spacing and aspect ratio of S and C shear surfaces are fractal on scales ranging from 10^3 μm to 1 km (Hippert 1999). Some strike-slip faults several hundreds of kilometers long transect entire mountain chains at low angles to the orogenic trend (e.g., North American Cordillera; see Figure 1 in Eisbacher 1985) and may represent C' surfaces (i.e., shear bands) at the largest scale. If so, the heterogeneities that promote strain localization on such long scales may reside in the upper mantle. Alternatively, they may reflect the distribution and amounts of metamorphic fluid and/or melt in the lower crust (Chapter 13).

Yardley and Baumgartner (Chapter 11) mention several mechanisms by which fluids can weaken rock, including hydrofracturing due to increased pore-fluid pressure, hydrolytic weakening of silicate minerals, or transformation of hard reactant minerals to intrinsically weak, hydrous mineral products (e.g., micas). Fluids released during prograde metamorphic reactions at depth may advect to sites of ongoing shearing, further weakening the rock and shortening the length scale of localization (see Chapter 4). The growth of mechanical instabilities may also be influenced by strain-dependent transitions in the active deformation mechanism(s), changes in the kinematics of deformation (i.e., shape of the strain ellipsoid, degree of noncoaxiality), or some combination of the above.

Two end-member scenarios describing the evolution of strain localization in a strike-slip fault system are illustrated in Figure 6.11. In strike-slip fault systems, most displacement is accommodated along a single master fault or a limited number of fault strands oriented parallel to the macroscopic shearing plane; only minor displacements are taken up by the surrounding complex of shear surfaces. The evolution of this geometry involves either increasing strain localization as the surrounding shear surfaces are deactivated and strain is concentrated on a narrow master fault (Figure 6.11a, homogenization of strain on a smaller scale than that of the initial fault array), or strain delocalization as shear surfaces making up an initially smaller fault array rotate, broaden, and coalesce to form the master fault (Figure 6.11b, homogenization of strain on the scale of the initial fault array). The former evolution, that is, "down-scaling" of strain homogeneity, has been observed in analogue studies of fault systems in brittle and elastoplastic materials (Tchalenko 1970) as well as in multi-layered, brittle-viscous composites (Schreurs 1994). "Up-scaling" of strain homogeneity has

(a) Downscaling

(b) Upscaling

Figure 6.11 Two end-member evolutions of strain localization: (a) down-scaling; (b) up-scaling.

been inferred from structural studies on natural shear zones (Fusseis et al. 2006) and observed on the granular scale in *in situ* deformation experiments (White et al. 1985). The implication of both types of strain evolution is that the relatively simple kinematic and dynamic boundary conditions of structurally mature fault systems justifies the extrapolation of laboratory-derived flow laws to the largest length scale at which shearing is homogeneous.

These structural observations provide a context from which to develop rheological models of large-scale fault systems. For continuum mechanical modeling of heterogeneous deformation, the challenge of modeling scale-dependent deformation is to define a representative elementary volume (REV), the smallest length scale or volume of rock that is statistically homogeneous. The REV comprises all constituent features of a rock that may be averaged and therefore treated as a structural and mechanical continuum on larger scales. Because rock is heterogeneous at scales smaller than that of the REV, the material parameters at larger scales must be determined from models that account for the properties of the components of the REV. Thus, the properties of the REV might be constrained by averaging the rheological parameters of the constituent phases. This would involve volume-weighting of the constituents' parameters, similar to the approach employed in modeling of polymineralic viscous aggregates (Tullis et al. 1991; Handy et al. 1999). In the case of heterogeneous shearing, however, the mechanical phases correspond not to different minerals but to sheared and less-sheared rock volumes with correspondingly different structures and rheologies (Handy 1994b).

What Is the Stress State in Shear Zones?

In situ stress measurements in deep boreholes indicate that the continental crust down to the FVT is at a critical or near-critical stress state at hydrostatic pore-fluid pressure (KTB borehole: Dresen et al. 1997; Zoback and Harjes 1997); that is, even small variations in the stress applied can lead to failure and a marked drop in strength. At the San Andreas Fault Observatory Drillhole (SAFOD), the measured stresses are consistent with those obtained from Byerlee's Law (Byerlee 1978, regime 3) for the thrust fault orientation in that area (Hickman and Zoback 2004). These observations suggest that brittle strength is invariant with length scale, at least over several orders of magnitude. However, it is unlikely that a measured stress state, critical or not, pertains to all length scales. For example, the anastomozing nature of all faults, above and below the FVT, indicates that yielding is attained only at some length scales and not at others. Therefore, criticality with regard to stress state appears to vary with time- and length scales of strain localization.

From the FVT downwards, differential stress estimates on the order of ~10–100 MPa are obtained from grain-size paleopiezometers for dynamically recrystallized quartz, and by extrapolating experimentally derived constitutive

relations for dislocation creep of quartz to natural strain rates (Etheridge and Wilkie 1981; Hirth et al. 2001; Stipp et al. 2002). Similar values have been obtained with identical methods for olivine-rich rocks of the upper mantle. These stress values are based on the assumption of mechanical and microstructural steady state for the length scale of observation (usually a thin section). In some cases, this assumption appears reasonable based on the preservation of relatively homogeneous microstructures at scales of 10–100 m (e.g., Dunlap et al. 1997). In other cases, however, microstructures preserve evidence of very large differential stress gradients on the millimeter scale (Handy 1994a).

The 10–100 MPa range cited above for rocks undergoing dislocation creep probably represents maximum, near-steady-state values, because any contribution from viscous granular flow mechanisms would reduce the creep strength, as inferred from microstructural studies in many shear zones. As mentioned above, such flow mechanisms are enhanced relative to dislocation creep when grain boundaries are pinned by phases produced during syntectonic reactions (Stünitz and Fitzgerald 1993). Most of the crustal faults sampled for paleo-piezometric studies are retrograde, amphibolite- and greenschist-facies shear zones. Their measured differential stress levels are probably greater than in higher grade shear zones, where high temperatures favor lower stresses. The extrapolation of experimental flow laws for power-law creep to temperatures at the base of the continental crust suggests that differential stresses there may be as low as 1–10 MPa, although nominally dry rocks (e.g., granulites) deforming at the same conditions may support flow stresses of an order of magnitude greater (e.g., Kohlstedt et al. 1995). This is corroborated by the observation of very fine (≤ 10 μm), dynamically recrystallized quartz and feldspar grains in granulites of the Ivrea-Verbano Zone, northern Italy (Zingg et al. 1990).

Prograde shear zones are rarely preserved in nature and usually cannot be used for paleopiezometry because post-tectonic grain growth has modified their stress-sensitive microstructures. Prograde shear zones probably accommodated crustal thickening at low temperature and/or high differential stress during initial burial. Only where stress and temperature drop very rapidly are prograde, stress-sensitive microstructures expected to be preserved (Knipe 1989). In general, it is a rock's thermal history and the mechanical response to that history which determine whether or not its dynamic microstructures are "frozen in."

Deviations from steady-state creep are expected over short timescales (<1000 yr) in the vicinity of active faults. As cited above, peak values of differential stress during coseismic faulting may be significantly higher than steady-state values. High transient stress during creep is consistent with evidence of rapid frictional melting and quenching in the form of pseudotachylite (rock glass) in some shear zones; the formation of pseudotachylite requires very fast (~ 1 m s^{-1}), short ($\leq$ s) bursts of movement at high shear strain rate ($\gamma = 1$–1000 s^{-1}) and shear stress ($\sim 10^2$ to 10^3 MPa; Otsuki et al. 2003).

The rate of stress change following rapid loading-unloading events (time interval t_2–t_3 in Figure 6.1) depends on the initial (peak) stress as well as on the strain, the creep parameters, and the ambient temperature of the host rock. Minimum rates of stress drop for the preservation of dynamically recrystallized quartz grain size in equilibrium with stress are about 10^{-9}–10^{-11} MPa s^{-1} (Prior et al. 1990), but much higher stress rates (and correspondingly large changes in strain rate) certainly occur, as manifested by stress-dependent microstructures in mylonite that have not equilibrated with differential stress (Küster and Stöckhert 1999; Trepmann and Stöckhert 2003). A key question from the standpoint of rheology is: How much strain and/or time are necessary for a state variable (e.g., grain size or dislocation density) to remain in equilibrium with stress after a change in deformational conditions? For example, when deformation is accommodated by subequal contributions of diffusion creep and dislocation creep, the grain-size evolution after a sudden change in deformational conditions controls the subsequent rheological evolution (Montesi and Hirth 2003).

Treatment of the lower continental crust as a heterogeneous viscous body emulates the stress memory of horizontally layered crust; a postseismic stress decay on the order of 10^{-7} MPa s^{-1} is obtained during the first 20 days after an assumed shock of M_w 7.3 (Ivins and Sammis 1996). Rapid viscous unloading of the lithosphere may occur in response to one or a combination of events: (a) the networking of large shear zones leading to the formation of an interconnected layer of weak rock; (b) the reaction of strong reactant phases, particularly phases deformed at physical conditions outside of their stability field, resulting in the production of intrinsically weak phases; (c) fluid influx reducing the effective stress, favoring brittle failure and stress release. In the case of (a), experimental and theoretical work on the rheology of polycrystalline aggregates indicates that the magnitude of weakening owing to networking depends on the interconnectivity of the weak phase and on its strength contrast with the surrounding, stronger phase (Handy et al. 1999). For two phases with a strength contrast of 5 : 1, for example, the interconnection of only 10 vol.-% of the weak phase reduces the strength of the entire rock by some 80%. However, shear zones do not always anastomoze completely and the entire lithosphere may not be cut by a single shear zone (e.g., Lister et al. 1991; Brun et al. 1994). Therefore, stress can remain very heterogeneous within the deforming lithosphere. In that case, bulk strength does not drop as far towards the uniform-stress lower bound and the strength of the system remains within 15–20% of the bulk strength of homogeneously deforming rock (Handy 1994b).

The mechanical response of the viscous crust to perturbations in stress and strain determines how stress is transferred through the lithosphere, both among shear zones below the FVT and back upwards to seismogenic fault zones in the brittle crust. To a first approximation, creep related to the downward propagation of a rupture surface into the viscous crust occurs just ahead of the surface and on either side of the surface at distances comparable to the depth of the seismogenic

zone (Mavko 1981; Montesi 2004). The time- and length scales of stress transfer in the viscous crust vary with viscosity, which in turn decreases with depth as a function of the geothermal gradient at a given background strain rate. The shorter the response time and the longer the length scale of stress transfer below the FVT, the greater the potential for shear zones to (re)load faults in the overlying brittle crust and therefore to trigger earthquakes. Stress transfer among brittle faults (Stein 1999) may be controlled in part by the viscous response of their ductile continuations below the FVT (e.g., Freed and Lin 2003).

What Do Measurements of Surface Deformation Tell Us about Rheology below the Frictional-to-Viscous Transition?

Large earthquakes or other deformation sources (e.g., volcanic intrusions, water reservoir fluctuations, or glacier surges) initiate a rock mechanics experiment of lithospheric dimensions in which a sudden stress change leads to a measurable relaxation of the lower crust and upper mantle. The surface motions related to faulting can be tracked with millimeter precision using space-based geodetic techniques—global positioning systems (GPS), very long baseline interferometry (VLBI), and synthetic aperture radar interferometry (InSAR). Thus, surface measurements provide a basis for testing structural and rheological models of the lithosphere below the FVT. Of course, motions at depth are filtered through the upper, brittle crust so that using them to resolve structure and constrain rheological parameters below the FVT is complicated by the fact that several deformational processes contribute to the observed motions.

Deformation rates during the interseismic period late in the earthquake cycle do not vary significantly with time and can be used to estimate long-term geologic slip rates (Savage and Burford 1970). First-order estimates of rheological parameters have been obtained by integrating geologic and geophysical information: paleoseismic constraints on the time since the last major earthquake, average earthquake repeat intervals, and geologic fault slip rate estimates, combined with estimates of the depth to the FVT from seismic or heat flow data can all be incorporated in a Bayesian statistical approach (Segall 2002; Johnson and Segall 2004; Hilley et al. 2005). In applying this approach to the Kunlun fault in northern Tibet, Hilley et al. (2005) showed that the viscosity of the lower crust may be at least an order of magnitude greater ($>10^{19}$ Pa s) than that estimated in channel flow models (10^{16}–10^{18} Pa s; e.g., Clark and Royden 2000). In another study using VLBI and GPS data from the southwestern U.S., Flesch et al. (2000) determined that effective, depth-averaged viscosity decreases by three orders of magnitude going from the Basin and Range area to the San Andreas fault system and the eastern California shear zone. Their estimates probably overestimate the real viscosity below the FVT, because they effectively equate strain rate with viscosity and therefore provide average viscosity estimates for the whole lithosphere.

Whether or not deformation is localized below the active FVT can be determined by comparing interseismic slip rates on aseismically moving fault segments with the overall, long-term displacement rate on those segments (Thatcher 1983). If deformation below the seismogenic zone is broadly distributed, then interseismic displacement rates should only be a fraction of the long-term rate. Accelerated motion following earthquakes on adjoining seismogenic fault segments would account for a significant portion of the long-term slip budget (Ben-Zion et al. 1993). However, observed rapid displacement rates along the central San Andreas and Hayward faults (California) approach their long-term slip rates, so deformation below the FVT is inferred to be quite localized (Bürgmann et al. 2000; Malservisi et al. 2002). A limitation of this approach is that the evolution of fault displacement rate on any given fault segment is affected by the activity of nearby seismogenic faults. Fault displacement therefore depends on the relaxation of time constants and distribution of transient viscous flow at depth (Schmidt 2002; Lynch et al. 2003).

Geodetic measurements of postseismic relaxation are more effective than interseismic displacement measurements for probing structure and rheology below the FVT. Interpretation of postseismic measurements in terms of rheology is hampered by the fact that several processes from different depths of a fault system contribute to the observed transient deformation. These include afterslip on narrow faults above (Bilham 1989; Bürgmann et al. 1997) and below (Tse and Rice 1986) the base of the seismogenic zone, viscous flow in the lower crust and upper mantle (Pollitz et al. 2000), and poroelastic rebound in the upper crust due to fluid flow in response to coseismic pressure changes (Peltzer et al. 1996; Jónsson et al. 2003). These effects are difficult to separate (Thatcher 1983; Savage 1990), especially for moderate to small earthquakes ($M_W < \sim 7$), where transient signals from below the FVT are difficult to distinguish from the multitude of shallow events (Bilham 1989; Pollitz et al. 1998; Jónsson et al. 2003). However, the signals are not as ambiguous when considering postseismic deformation near large strike-slip ruptures with a well-defined, finite length (Pollitz et al. 2000) or faults with a significant dip-slip component (Pollitz et al. 1998; Hsü et al. 2002).

Comparison of three-dimensional ground motions associated with large strike-slip earthquakes indicates that the style of deformation below the seismic–aseismic transition varies with lithology, lithospheric structure, and thermal regime. For example, the pattern of deformation after the 1992 $M_W = 7.3$ Landers, 1999 $M_W = 7.1$ Hector Mine earthquake sequence in the Mojave Desert of the southwestern U.S. (Figure 6.12) suggests that poroelastic rebound predominated in the upper crust (Peltzer et al. 1996), whereas viscous flow below the coseismic rupture was probably localized in the lower crust (Fialko 2004) and/or upper mantle (Pollitz et al. 2000, 2001; Freed and Bürgmann 2004). Freed and Bürgmann (2004) fit the spatial and temporal patterns in the GPS data following both earthquakes with a model that relied on experimentally
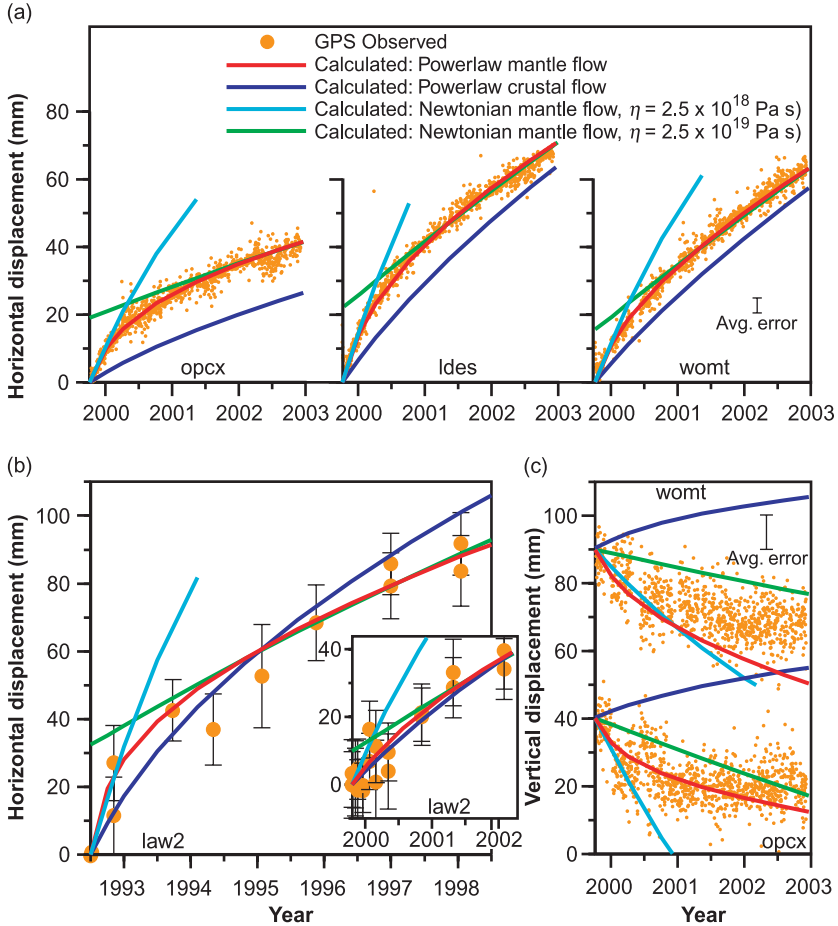
Figure 6.12 Observed and calculated postseismic displacement time series following the 1992 Landers and 1999 Hector Mine earthquakes (from Freed and Bürgmann 2004): (a) horizontal displacements at three continuously monitored GPS stations following the 1999 Hector Mine earthquake; (b) horizontal displacements at campaign GPS station law2 following the 1992 Landers earthquake. Inset shows campaign data at law2 following the Hector Mine earthquake; (c) vertical motions at two continuously monitored stations following 1999 Hector Mine earthquake. The power-law mantle flow model (red curves) is valid for an aplitic lower crust, a mantle with the rheology of nominally wet olivine (Hirth and Kohlstedt 2003), and a geotherm near the upper bound permitted ($T_{40km} = 1225°C$) by heat flow data. Neither the power-law crustal model (blue curves), which assumes wet quartzite in the lower crust and a cooler dry olivine mantle ($T_{40\_km} = 1100°C$), nor any models that assume dominant creep in the lower crust, fit the vertical motion data. The Newtonian models incorporate mantle flow with a low viscosity (2.5×10^{18} Pa s, cyan curves) and an order-of-magnitude greater viscosity (green curves) that match early and late time series slopes, respectively.

determined nonlinear viscous creep parameters of nominally wet olivine (Hirth and Kohlstedt 2003) at temperatures consistent with surface heat-flow measurements (Figure 6.12). In light of microstructural evidence for viscous granular flow in naturally deformed lower crustal and upper mantle rocks (e.g., Jaroslow et al. 1996; Stünitz and Fitzgerald 1993; Handy and Stünitz 2002), it is interesting to consider whether the same GPS data could be modeled with a composite dislocation creep-diffusion creep rheology in which the average grain size evolves with time (e.g., Montesi and Hirth 2003). Grain growth at high homologous temperatures is likely in fine-grained aggregates produced by high coseismic stresses.

Irrespective of the creep mechanisms, the lower crust beneath the earthquakes appears to contribute little to the postseismic transients of the first few years, suggesting that Mojave Desert crust comprises relatively mafic and/or dry lithologies. Thus, the viscous contribution to relaxation following the Landers–Hector Mine earthquake sequence appears to originate from flow of a hot, possibly wet asthenospheric mantle—a conclusion also reached for the 2002 $M_W = 7.8$ Denali earthquake in southern Alaska (Bürgmann et al. 2003). Both of these earthquakes occurred in broad, active plate-boundary settings that lack the deep lithospheric root found beneath cratonic, continental interiors (Dixon et al. 2004; Hyndman et al. 2005).

In contrast to the cases above, very localized shearing extending below the coseismic rupture to depths of 35 km to the base of the crust is inferred from surface deformation following the 1999 $M_W \approx 7.4$ Izmit earthquake along the North Anatolian fault in Turkey (Bürgmann et al. 2002). A velocity-strengthening frictional rheology or a tabular zone of very low effective viscosity in the lower crust provides good fits to the observed surface motions (Hearn et al. 2000). A similar conclusion was reached by Kenner and Segall (2003) based on modeling of several decades-old accelerated postseismic surface deformation following the 1906 $M_W \approx 7.7$ San Andreas fault earthquake. Likewise, Johnson and Segall (2004) found that deformation data in northern and southern California are best fit by a single model parameterization, combining a lower crustal, aseismic shear zone beneath the San Andreas fault with an underlying viscous mantle. This is qualitatively consistent with evidence for distributed shear in the upper mantle from shear wave splitting (Hartog and Schwartz 2001) and magnetotelluric studies (Maerklin et al. 2005).

With the exception of studies of subduction zone events, there are few well-studied postseismic deformation studies for thrust faults and normal faults. Two earthquake studies thus far illustrate differences in the surface response to thrusting in differently aged, convergent settings: a young active fold-and-thrust belt in Taiwan versus intraplate deformation of a cold, thick cratonic lithosphere on the Indian peninsula. In the former case, rapid and extensive surface deformation following the $M_W = 7.8$ Chi-Chi thrust earthquake in Taiwan indicates the strong contribution of afterslip extending down-dip from the base of the coseismic

rupture surface (Hsü et al. 2002), possibly into the viscous crust. In contrast, the equally large 2001 Bhuj intraplate thrust earthquake, a deep event located in a reactivated Proterozoic rift structure in northwestern India, was followed by only minor transient deformation in the first six months (Jade et al. 2002).

Normal faulting during the 1959 Hebken Peak earthquake in the northern Basin and Range province (southwestern U.S.) led to broad postseismic uplift that is consistent with viscous relaxation in the upper mantle, but not with lower crustal relaxation or localized afterslip in the viscous crust down-dip of the rupture (Nishimura and Thatcher 2003). These results are consistent with other analyses of lithospheric rheology in the Basin and Range province based on deformation associated with reservoir impoundment (Kaufmann and Amelung 2000) and Holocene rebound of shorelines along Lake Bonneville (Bills et al. 1994).

Mineralogy, geothermal gradient, and fluid availability govern the rheology of the lithosphere, and thus the nature of deformation during the earthquake cycle. Where the bulk viscous rheology below the FVT is nonlinear, as suggested by surface deformation studies and microstructural studies of exhumed mylonitic rocks, viscosities can be highly stress and, hence, time dependent. A strong time dependence of bulk viscosity is also expected for lithosphere containing networks of fine-grained mylonitic rocks undergoing viscous granular creep, especially if syntectonic grain size increases with time during the post- and interseismic intervals (Montesi and Hirth 2003). Thus, effective viscosities determined by measurements of surface deformation at various stages of postseismic deformation cannot be directly compared, either with each other or to estimates derived from long-term geologic features. Better and more data are needed to constrain fully the evolution of postseismic deformation in time and space.

Owing to the relatively small strains during postseismic deformation, it is unclear how much of the deformational response measured at the Earth's surface is accommodated by transient creep processes. For example, experimental work indicates that although the temperature and stress dependence of high-temperature transient creep in olivine is similar to that of steady-state creep, the effective viscosity may be a factor of 2–5 less (Chopra 1997). A promising approach for understanding the physics of transient creep involves formulating equations of state that bridge the gap between steady-state and transient creep processes (Stone et al. 2004). This may significantly improve our ability to relate creep rates inferred from geodetic measurements to deformational conditions recorded by microstructures in exhumed fault rocks.

How Is Decoupling across Mechanical Interfaces Related to Strain Partitioning in the Lithosphere?

"Coupling" and "decoupling" are widely used and misleading terms because they mean different things to different specialists. In geological parlance, decoupling refers to discontinuities in a velocity field, manifested as a

displacement of markers across a surface (i.e., a fault or shear zone). As noted in the discussion of Figure 6.1, faulting can involve episodic decoupling. The degree of decoupling can be defined as the ratio of displacement on a fault to the total displacement accommodated by the system (fault plus adjacent rock) over a specified time interval. This definition obviously depends on the time- and length scales of observation. By contrast, in seismological parlance, "seismic coupling" refers to the proportion of total displacement on a surface accommodated by coseismic movement. Here, confusion arises because decoupling zones (in a geological context) during an earthquake are referred to by seismologists as seismic coupling zones.

Similarly, "partitioning" is a kinematic term describing the division of a far-field strain or displacement field into different vectorial components on a system of variably oriented faults (discussion in Dewey et al. 1998). Partitioning necessarily involves decoupling, but not all decoupling surfaces partition displacement. Displacements on faults that are coincident with the overall displacement field are said to be unpartitioned. These definitions are important when attempting to draw mechanical inferences from displacement fields.

First-order decoupling surfaces within the continental lithosphere are the sediment–basement contact, the FVT, the crust–mantle boundary, and, where present, the boundary between the base of the hydrous quartz-rich crust and the mafic lower crust (Handy and Brun 2004). These are inferred to be weak horizons within the lithosphere. However, either coupling or decoupling, in the absence of partitioning between the continental crust and upper mantle, is required to explain nearly coincident displacement fields for the surface and the upper mantle inferred from geodetic and seismic anisotropy data in eastern Tibet (Holt 2000). In subduction zone systems, the relationship between plate kinematics and fault displacements is more complex: oblique convergence between lithospheric plates is partitioned into thrusting at high angles to the plate boundary on low-angle megathrusts and strike-slip motion on trench-parallel faults within the magmatic arc (Fitch 1972; Jarrard 1986).

Rheological models incorporating time-dependent brittle behavior of the upper crust predict that, while viscous creep prevails at depths below about 15 km, fault motion above this level is punctuated by episodic, coseismic displacement (Figure 6.1). In the case of strike-slip faulting, such models adopt two, end-member, dynamic-kinematic boundary conditions: lateral drive, in which forces are exerted by the opposite motion of blocks on either side of the fault (e.g., Tse and Rice 1986), and basal drive involving drag of the blocks from below by creep of a viscous substratum (e.g., Li and Rice 1987). Molnar (1992) argued that viscous creep of the lower crust transmits displacements from the strong, ductile upper mantle to the upper, brittle crust, while smoothing displacement discontinuities between these two layers. He inferred the lower depth limit of strain partitioning in the crust to be the interface between brittle and viscous crustal domains (the FVT) because flow of the weak, viscous crust causes the

principle stress axes to be nearly orthogonal to the horizontal base of the overlying crustal blocks. Still, most rocks in the lithosphere are strongly anisotropic and folding of anisotropies below the FVT can cause the principal stress axes to be oblique to both compositional layering on the lithospheric scale and to shear zones aligned parallel to the FVT. Strain continuum models (Bourne et al. 1998; Teyssier et al. 2002) predict that intracrustal strain is accommodated within zones of distributed, three-dimensional strain at the top of the viscous crust. The thickness and geometry of these accommodation zones depends presumably on the degree of coupling at the FVT, which in the continuum models is simply assumed to be complete. These end-member models shed valuable light on some, but not all, aspects of strain accommodation at mechanical interfaces in the lithosphere. The dilemma remains whether strain compatibility in the lithosphere is maintained by coseismic decoupling, by continuous coupling and three-dimensional flow, or by some combination of these scenarios.

A possible solution to this dilemma is that mature shear zone systems comprise zones of decoupling which develop, usually in previously foliated rocks, in response to strain incompatibilities between adjacent lithospheric blocks. Structural studies reveal that the geometry of networked, shear zone systems in foliated rocks reflects both the flow vorticity and the shape of the finite strain ellipsoid (Figure 6.13a; Gapais et al. 1987). The orientations of mylonitic foliations and stretching lineations in natural fault systems support the prediction of slip-line theory for anisotropic materials (Cobbold and Gapais 1986) that active shear zones track (but do not exactly coincide with) surfaces of no finite extension within the bulk strain ellipsoid, whereas their lineations track directions of maximum shear within this ellipsoid (Figure 6.13b). These fabric orientations correspond to the shearing plane and principal finite strain axes only for simple strain configurations (e.g., simple shearing, coaxial flattening, Figure 6.13b) at high strains. For more general, three-dimensional strain states, they are oriented obliquely to the shearing plane. The attainment of these stable orientations for foliations and stretching lineations involves several possible mechanisms: from the growth and/or rigid body rotation of platy minerals (e.g., mica) to the buckling and shearing of layers, as discussed in the previous section.

Strain partitioning and fabric asymmetry related to decoupling at and below the FVT are shown in Figure 6.14, which summarizes the deep structure of the Periadriatic fault system in the Central Alps as exposed today at Earth's surface. As described by Furlong et al. (Chapter 4), this fossil fault system is an excellent natural laboratory for studying deep-seated processes. Oblique shortening is accommodated by a network of kilometer-scale shear zones and folds that nucleated at existing nappe contacts, and especially along the surface of the rigid, cold orogenic block. When analyzed with the slip-line method, the orientation of this network with respect to the cold indenter block (equal area projections in Figure 6.14) is consistent with dextral transpression and exhumation of the
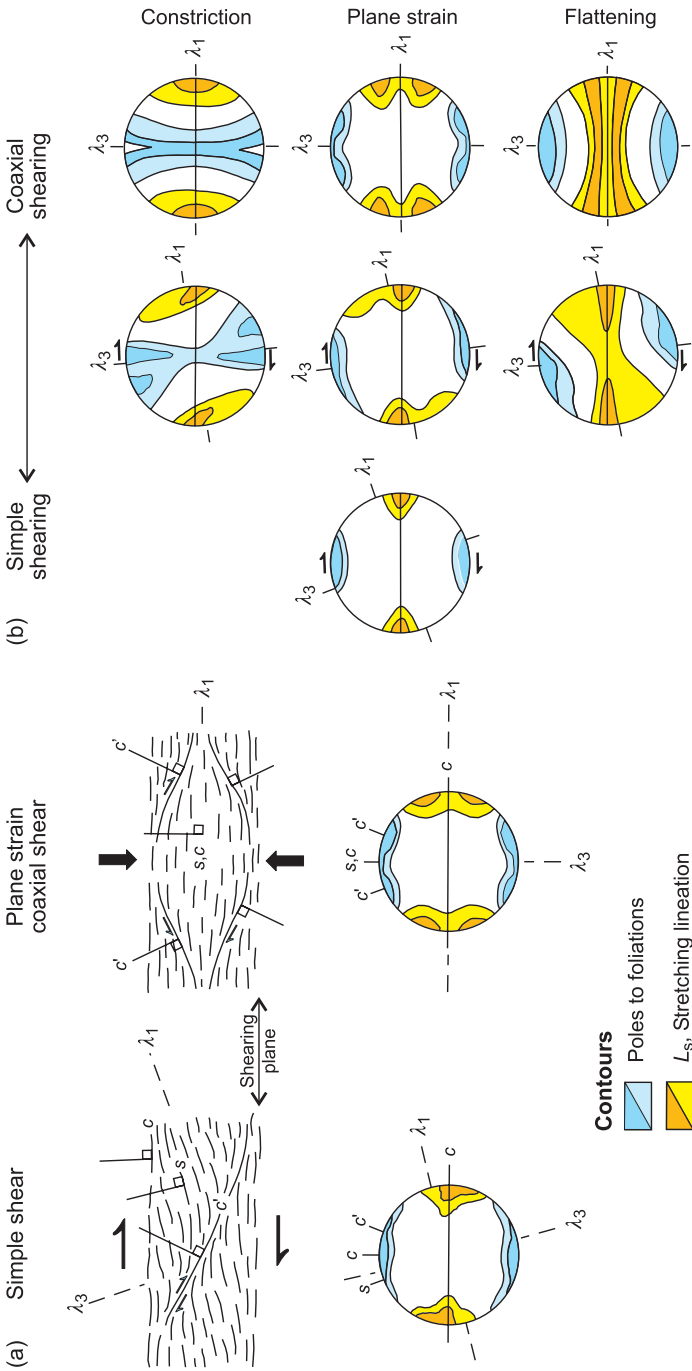
Figure 6.13   Structures and orientation distribution patterns for shear zones predicted by slip-line theory: (a) bulk simple shearing (left) and plane-strain coaxial shearing (right) with diagnostic pole patterns: black, gray = poles to mylonitic foliations (S, C, C'); hatched, dark gray = stretching lineations; (b) equal-area projections of predicted preferred fabric orientations for various finite strains and deformational histories. λ_1, λ_3 are the greatest and least principal quadratic stretching directions. Figure modified from Figure 14 of Gapais and Cobbold (1987).
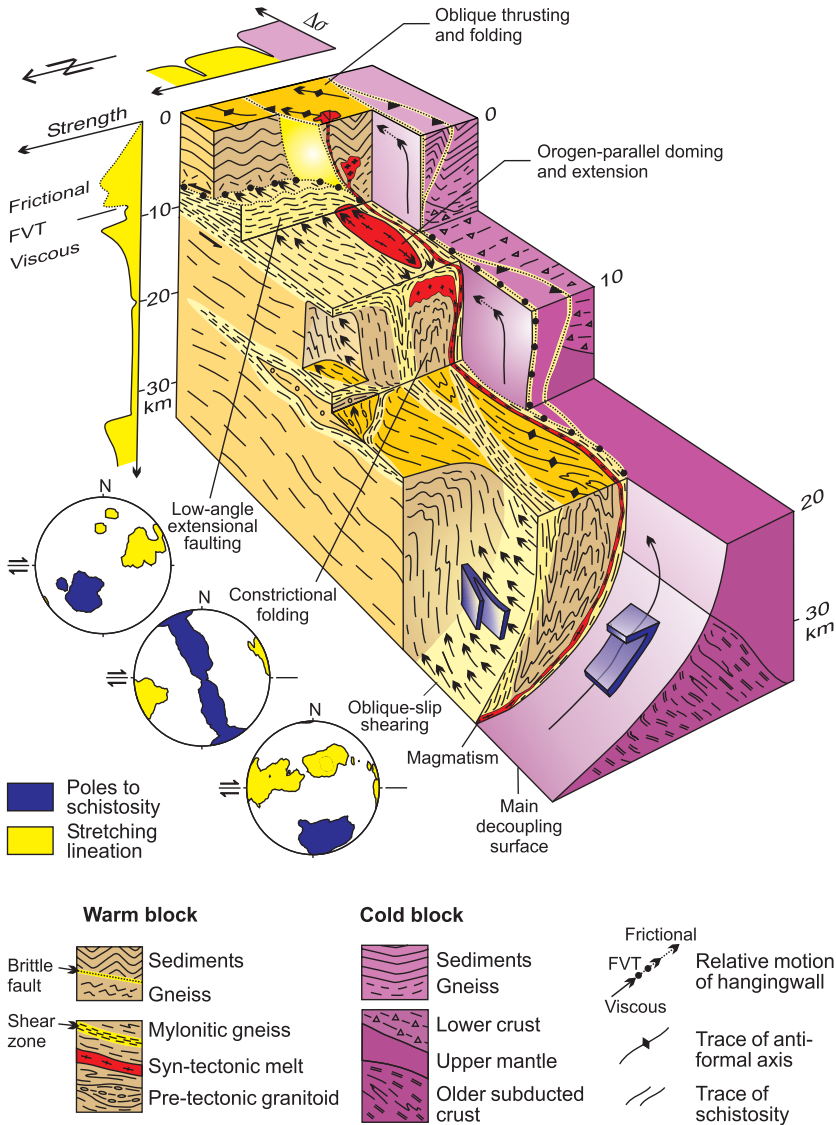
Figure 6.14 Generic model of decoupling zones related to strain partitioning along the transpressive Periadriatic fault system (modified from Handy et al. 2005). The equal area projections (bottom left) contain planar and linear fabrics in the warm block.

warm orogenic block (Handy et al. 2005). These kinematically linked structures thus serve as vertical and horizontal decoupling horizons, partitioning strain and transferring stress from the upper mantle to the upper crust.

We note that the symmetry of the foliation and stretching lineation orientations predicted with the Cobbold–Gapais slip-line model is never lower than monoclinic, even in general three-dimensional strain fields. This contrasts with the triclinic fabric symmetries predicted for some transpressional and transtensional configurations by strain continuum models in which the foliation and lineation are assumed to be passive markers (Fossen and Tikoff 1998; Lin et al. 1998). In these models, fabrics tend to rotate toward so-called fabric attractors, that is, directions for which the rates of particle motion are lowest. Yet, despite the simple assumptions of the slip-line model (simple shearing parallel to inextensible anisotropies, no strain hardening, no mechanical control on shear zone initiation and propagation), the fact that it incorporates anisotropies which can rotate and/or grow at each other's expense renders it arguably more realistic than existing, more complex three-dimensional strain models for homogeneous materials. Excepting some high-grade shear zones in which strength contrasts are presumably negligible, most natural rocks have one or more anisotropies (schistosity, compositional layering) comprising minerals with contrasting rheologies.

The Cobbold–Gapais model has several implications for coupling and strain partitioning in the lithosphere. First, strain partitioning is not restricted to the brittle crust; it potentially occurs in all foliated rocks of the lithosphere. Second, decoupling and strain partitioning are complementary phenomena on the time- and length scales of deformation in the viscous crust; shear strength is reduced, but never totally lost during the networking of shear zones. Finally, the orientation of structures in shear zones yields information about the strain and stress history during localization (Figure 6.13b).

These ideas pertain to the crust and upper mantle, but little is known about decoupling and strain partitioning at the interface of the lithosphere and asthenosphere. As imaged by current geophysical methods (see Chapter 2), shear zones in the upper mantle appear to be homogeneous shear zones some 100–200 km wide (Vauchez and Tommasi 2003). However, shear zones active in the upper mantle that have been mapped in exhumed mantle rocks are much narrower (widths from millimeters to hundreds of meters, e.g., Drury et al. 1991; Vissers et al. 1995; Handy and Stünitz 2002), indicating that current imaging methods are unable to resolve all length scales of localization in the mantle (see Chapter 4). Large strike-slip faults at the surface can be traced down to the upper mantle, where they are discernable as offsets in P-wave velocity anomalies at depths of 170 km (Wittlinger et al. 1996). Whereas fault geometry and kinematics in the lithosphere reflect the motion of tectonic plates, faults at the base of the lithosphere may develop in response to motion of the asthenosphere. Numerical models of convective overturn in a closed and coupled lithosphere–asthenosphere system indicate that surface displacement fields and faults may be kinematically linked to the boundaries of rapidly convecting mantle masses (Trompert and Hansen 1998).

CONCLUSIONS

Faults evolve on different time- and length scales. As such, faults must be considered as multicomponent systems that comprise one or more mechanical instabilities (weakened rock) and their surroundings (adjacent rock, the erosional surface). Faults nucleate on existing mechanical heterogeneities in the lithosphere, but it is still not clear why mechanical instabilities develop faster and grow longer on some length scales and not on others. Several factors influence the growth of instabilities, primarily the nature of stress interaction between existing heterogeneities. This interaction is itself a function of the geometry and spacing of these heterogeneities, the time- and rate-dependent rheology of the intervening rock, as well as the ambient, far-field stress state.

The rheology of fault rocks is more than just the relationship between the tensors of stress and incremental strain or strain rate; it includes aspects of rock history, such as the compositional, thermal, and structural characteristics of the rock. In general, the longer the time- and length scales of faulting considered, the greater the potential influence of the kinematic and thermal history on the rheology of the fault system.

Fracturing and folding-plus-mylonitization are the main modes of strain localization, respectively, above and below the FVT. These modes operate over the same large range of length scales, but on very different timescales, reflecting the different grain-scale mechanisms (cataclasis, creep) controlling these processes. At the FVT, localization processes are strain dependent and rate competitive; brittle and viscous mechanisms contribute subequally to the bulk strain and strain rate if regarded on sufficiently long time- and length scales. Still, fault systems never achieve mechanical steady state in their entirety. This pertains especially to parts of faults at and near the FVT, where brittle, sometimes seismic instabilities perturb the ambient stress field on timescales ranging from seconds to years. As a consequence, the notion that the crust is at a critical state of failure may only apply to length scales related to those of existing mechanical heterogeneities, and on timescales related to the mechanical response time of the crust.

Fault geometry simplifies with progressive strain, lending justification to the use of laboratory-derived flow laws to estimate the bulk rock rheology on length scales at which strain is homogeneous. The rheology of larger or smaller rock bodies for which strain is heterogeneous can be modeled either as a two-phase aggregate or a representative size or volume within which the mechanical properties of the system are statistically homogeneous. In general, the kinematics of faulting and fault geometry are as important as grain-scale deformation mechanisms in determining the rheology of fault systems on the lithospheric scale. This is consistent with observations and theoretical predictions that shear zone structures (foliations, stretching lineations) attain orientations which reflect the kinematic vorticity and the shape of the finite strain ellipsoid. Shear zones are therefore zones of strain accommodation that transmit shear stress within the lithosphere.

ACKNOWLEDGMENTS

REFERENCES

Austrheim, H., and T.M. Boundy. 1994. Pseudotachylites generated during seismic faulting and eclogization of the deep crust. *Science* **265**:82–83.

Bauer, P., S. Palm, and M.R. Handy. 2000. Strain localization and fluid pathways in mylonite: Inferences from in-situ deformation of a water-bearing quartz analogue (norcamphor). *Tectonophysics* **320**:141–165.

Ben-Zion, Y., J.R. Rice, and R. Dmowska. 1993. Interaction of the San Andreas fault creeping segment with adjacent great rupture zones and earthquake recurrence at Parkfield. *J. Geophys. Res.* **98**:2135–2144.

Berthé, D., P. Choukroune, and D. Gapais. 1979. Orientations préférentielles du quartz et orthogneissification progressive en régime cisaillant: L'exemple du cisaillement Sud-Armoricain. *Bull. Minéral.* **102**:265–272.

Bilham, R. 1989. Surface slip subsequent to the 24 November 1987 Superstition Hills, California, earthquake monitored by digital creepmeters. *Bull. Seismol. Soc. Am.* **79**:424–450.

Bills, B.G., D.R. Currey, and G.A. Marshall. 1994. Viscosity estimates for the crust and upper mantle from patterns of lacustrine shoreline deformation in the Eastern Great Basin. *J. Geophys. Res.* **99**:22,059–22,086.

Bos, B., C.J. Peach, and C.J. Spiers 2000. Frictional–viscous flow of simulated fault gouge caused by the combined effects of phyllosilicates and pressure solution. *Tectonophysics* **327**:173–194.

Bos, B., and C.J. Spiers. 2002. Frictional–viscous flow of phyllosilicate-bearing fault rock: Microphysical model and implications for crustal strength profiles. *J. Geophys. Res.* **107**:B2, 1–13.

Bouchon, M. 1997. The state of stress on some faults of the San Andreas system as inferred from near-field strong motion data. *J. Geophys. Res.* **102**:11,731–11,744.

Bourne, S.J., P.C. England, and B. Parsons. 1998. The motion of crustal blocks driven by flow of the lower lithosphere and implications for slip rates of continental strike-slip faults. *Nature* **391**:655–659.

Brace, W.F., and D.L. Kohlstedt. 1980. Limits on lithospheric stress imposed by laboratory experiments. *J. Geophys. Res.* **85**:B11, 6248–6252.

Brodie, K.H., and E.H. Rutter. 1985. On the relationship between deformation and metamorphism with special reference to the behavior of basic rocks. In: Kinematics, Textures, and Deformation: Advances in Physical Geochemistry, ed. A.B. Thompson and D. Rubie, pp. 138–179. Berlin: Springer Verlag.

Brodie, K.H., and E.H. Rutter. 1987. The role of transiently fine-grained reaction products in syntectonic metamorphism. *Canad. J. Earth Sci.* **24**:556–564.

Brun, J.P., D. Sokoutis, and J. Driessche. 1994. Analogue modeling of detachment fault systems and core complexes. *Geology* **22**:319–322.

Bürgmann, R., E. Calais, A.M. Freed, J. Freymueller, and S. Hreinsdóttir. 2003. Mechanics of postseismic deformation following the 2002, $M_w = 7.9$, Denali fault earthquake. *EOS Trans. AGU* **84**.

Bürgmann, R., S. Ergintav, P. Segall et al. 2002. Time-dependent distributed afterslip on and deep below the Izmit earthquake rupture. *Bull. Seismol. Soc. Am.* **92**:126–137.

Bürgmann, R., D. Schmidt, R. Nadeau et al. 2000. Earthquake potential along the northern Hayward fault. *Science* **289**:1178–1182.

Bürgmann, R., P. Segall, M. Lisowski, and J. Svarc. 1997. Postseismic strain following the 1989 Loma Prieta earthquake from GPS and leveling measurements. *J. Geophys. Res.* **102**:4933–4955.

Byerlee, J.D. 1978. Friction of rocks. *Pure & Appl. Geophys.* **116**:615–626.

Chester, F.M. 1988. The brittle–ductile transition in a deformation mechanism map for halite. *Tectonophysics* **154**:125–136.

Chopra, P.N. 1997. High-temperature transient creep in olivine rocks. *Tectonophysics* **279**:93–111.

Clark, M.K., and L.H. Royden. 2000. Topographic ooze: Building the eastern margin of Tibet by lower crustal flow. *Geology* **28**:703–706.

Cobbold, P.R. 1977. Description and origin of banded deformation structures. II. Rheology and the growth of banded perturbations. *Canad. J. Earth Sci.* **14**:2510–2523.

Cobbold, P.R., and D. Gapais. 1986. Slip-system domains. I. Plane-strain kinematics of arrays of coherent bands with twinned fibre orientations. *Tectonophysics* **131**:113–132.

Dell Angelo, L.N., and J. Tullis. 1996. Textural and mechanical evolution with progressive strain in experimentally deformed aplite. *Tectonophysics* **256**:57–82.

Dewey, J.F., R.E. Holdsworth, and R.A. Strachan. 1998. Transpression and transtension zones. In: Continental Transpressional and Transtensional Tectonics, Spec. Publ. 135, pp. 1–14. London: Geol. Soc.

Dixon, J.E., T.H. Dixon, D.R. Bell, and R. Malservisi. 2004. Lateral variation in upper mantle viscosity: Role of water. *Earth Planet. Sci. Lett.* **222**:451–467.

Dresen, G., J. Duyster, B. Stöckhert, R. Wirth, and G. Zulauf. 1997. Quartz dislocation microstructure between 7000 m and 9100 m depth from the Continental Deep Drilling Program KTB. *J. Geophys. Res.* **102**:B8, 18,443–18,452.

Drury, M.R., R.L.M. Vissers, D. Van der Wal, and E.H. Hoogerduijn Strating. 1991. Shear localisation in upper mantle peridotites. *Pure & Appl. Geophys.* **137**:439–460.

Dunlap, W.J., G. Hirth, and C. Teyssier. 1997. Thermomechanical evolution of a midcrustal duplex and implications for midcrustal rheology. *Tectonics* **16**:983–1000.

Dutruge, G., J.-P. Burg, and J. Lapierre. 1995. Shear strain analysis and periodicity within shear gradients of metagranite shear zones. *J. Struct. Geol.* **17**:819–830.

Eisbacher, G.H. 1985. Pericollisional strike-slip faults and synorogenic basins, Canadian Cordillera. In: Strike-Slip Deformation, Basin Formation, and Sedimentation, ed. K.T. Biddle and N. Christie-Blick, SEPM Spec. Publ. 37, pp. 265–282. Tulsa, OK: Soc. Economic Paleontologists and Mineralogists.

Etheridge, M.A. 1983. Differential stress magnitudes during regional deformation and metamorphism: Upper bound imposed by tensile fracturing. *Geology* **11**:232–234.

Etheridge, M.A., and J.C. Wilkie. 1981. An assessment of dynamically recrystallized grain size as a paleopiezometer in quartz-bearing mylonite zones. *Tectonophysics* **78**:475–508.

Fialko, Y. 2004. Evidence of fluid-filled upper crust from observations of postseismic deformation due to the 1992 M_w 7.3 Landers earthquake. *J. Geophys. Res.* **109**:B08401, doi: 10.10129/2004JB002985.

Fitch, T.J. 1972. Plate convergence, transcurrent faults, and internal deformation adjacent to southeast Asia and the western Pacific. *J. Geophys. Res.* **77**:4432–4460.

Flesch, L.M., W.E. Holt, A.J. Haines, and B. Shen-Tu. 2000. Dynamics of the Pacific–North American plate boundary in the United States. *Science* **287**:834–836.

Fossen, H., and B. Tikoff. 1998. Extended models of transpression and transtension, and application to tectonic settings. In: Continental Transpressional and Transtensional Tectonics, ed. J.F. Dewey, R.E. Holdsworth, and R.A. Strachan. Spec. Publ. 135, pp. 15–33. London: Geol. Soc.

Fredrich, J.T., B. Evans, and T.-F. Wong. 1989. Micromechanics of the brittle to plastic transition in Carrara marble. *J. Geophys. Res.* **94**:4129–4145.

Freed, A.M., and R. Bürgmann. 2004. Evidence of powerlaw flow in the Mojave Desert mantle. *Nature* **430**:548–551.

Freed, A.M., and J. Lin. 2002. Accelerated stress buildup on the southern San Andreas fault and surrounding regions caused by Mojave Desert earthquakes. *Geology* **30**:6, 571–574.

Fusseis, F., M.R. Handy, and C. Schrank. 2006. Networking of shear zones at the brittle-to-viscous transition (Cap de Creus, NE Spain). *J. Struct. Geol.* **28**:228–1243.

Gapais, D., P. Bale, P. Choukroune et al. 1987. Bulk kinematics from shear zone patterns: Some field examples. *J. Struct. Geol.* **9**:635–646.

Gapais, D., and P.R. Cobbold. 1987. Slip system domains. 2. Kinematic aspects of fabric development in polycrystalline aggregates. *Tectonophysics* **138**:289–309.

Green, H.W., II, and P.C. Burnley. 1990. The failure mechanism for deep-focus earthquakes. In: Deformation Mechanisms, Rheology and Tectonics, ed. R.J. Knipe and E.H. Rutter. Geological Soc. Spec. Publ. London: 54. Geological Soc. pp. 133–141.

Hacker, B.R., S.M. Peacock, G.A. Abers, and S.D. Holloway. 2003. Subduction factory 2. Are intermediate-depth earthquakes in subducting slabs linked to metamorphic dehydration reactions? *J. Geophys. Res.* **108**:B1, doi: 10.1029/2001JB001129.

Handy, M.R. 1989. Deformation regimes and the rheological evolution of fault zones in the lithosphere: The effects of pressure, temperature, grain size, and time. *Tectonophysics* **163**:119–152.

Handy, M.R. 1994a. Flow laws for rocks containing two nonlinear viscous phases: A phenomenological approach. *J. Struct. Geol.* **16**:287–301.

Handy, M.R. 1994b. The energetics of steady state heterogeneous shear in mylonitic rock. *Mater. Sci. & Engin.* **A174**:261–272.

Handy, M.R. 1998. Fault rocks from an exhumed intracrustal extensional detachment: The Pogallo ductile fault zone. In: Fault-related Rocks: A Photographic Atlas, ed. A.W. Snoke, J.A. Tullis, and V.R. Todd, pp. 164–169. Princeton: Princeton Univ. Press.

Handy, M.R., J. Babist, R. Wagner, C. Rosenberg, and M. Konrad. 2005. Decoupling and its relation to strain partitioning in continental lithosphere: Insight from the Periadriatic fault system (European Alps). In: Deformation Mechanisms, Rheology and Tectonics: From Minerals to the Lithosphere, ed., D. Gapais, J.-P. Brun, and P.R. Cobbold, Spec. Publ. 243, pp. 249–276. London: Geol. Soc.

Handy, M.R., and J.-P. Brun. 2004. Seismicity, structure, and strength of the lithosphere. *Earth Planet. Sci. Lett.* **223**:427–441.

Handy, M.R., and H. Stünitz. 2002. Strain localization by fracturing and reaction weakening: A mechanism for initiating exhumation of subcontinental mantle beneath rifted margins. In: Deformation Mechanisms, Rheology and Tectonics: Current Status and Future Perspectives, ed. S. de Meer, M.R. Drury, J.H.P. de Bresser, and G.M. Pennock. Geological Society, Spec. Publ. 200, pp. 387–407. London: Geol. Soc.

Handy, M.R., S.B. Wissing, and J.E. Streit. 1999. Frictional-viscous flow in mylonite with varied bimineralic composition and its effect on lithospheric strength. *Tectonophysics* **303**:175–191.

Hartog, R., and S.Y. Schwartz. 2001. Depth-dependent mantle anisotropy below the San Andreas fault system: Apparent splitting parameters and waveforms. *Geophys. Res. Lett.* **106**:4155–4167.

Hearn, E.H., R. Bürgmann, and P. Reilinger. 2002. Dynamics of Izmit earthquake postseismic deformation and loading of the Duzce earthquake hypocenter. *Bull. Seismol. Soc. Am.* **92**:172–193.

Hickman, S., and M. Zoback. 2004. Stress orientations and magnitudes in the SAFOD pilot hole. *Geophys. Res. Lett.* **31**:L15S12, doi:10.1029/2003GL020043.

Hilley, G.E., R. Bürgmann, P. Molnar, and P. Zhang. 2005. Bayesian inference of plastosphere viscosities near the Kunlun Fault, northern Tibet. *Geophys. Res. Lett.* **32**:L01302, doi:10.1029/2004GL021658.

Hippert, J. 1999. Are S-C structures, duplexes, and conjugate shear zones different manifestations of the same scale-invariant phenomenon? *J. Struct. Geol.* **21**: 975–984.

Hirth, G., and D.L. Kohlstedt. 2003. Rheology of the upper mantle and the mantle wedge: A view from the experimentalists, in: Inside the Subduction Factory, ed. J. Eiler, Geophys. Monogr. Ser. 138, pp. 83–105. Washington, D.C.: Am. Geophys. Union.

Hirth, G., C. Teyssier, and W.J. Dunlap. 2001. An evaluation of quartzite flow laws based on com-parisons between experimentally and naturally deformed rocks. *Intl. J. Earth Sci.* **90**:77–87.

Hirth, G., and J. Tullis. 1994. The brittle–plastic transition in experimentally deformed quartz aggregates. *J. Geophys. Res.* **99**:11,731–11,747.

Hobbs, B.E., H.-B. Mühlhaus, and A. Ord. 1990. Instability, softening, and localization of deformation. In: Deformation Mechanisms, Rheology, and Tectonics, ed. R.J. Knipe and E.H. Rutter, Spec. Publ. 54, pp. 143–165. London: Geol. Soc.

Hobbs, B.E., A. Ord, and C. Teyssier. 1986. Earthquakes in the ductile regime? *Pure & Appl. Geophys.* **124**:309–336.

Holt, W.E. 2000. Correlated crust and mantle strain fields in Tibet. *Geology* **28**:67–70.

Hsu, Y.J., N. Bechor, P. Segall et al. 2002. Rapid afterslip following the 1999 Chi-Chi, Taiwan earthquake. *Geophys. Res. Lett.* **29**:16, doi:10.1029/2002GL014967.

Hyndman, R.D., C.A. Currie, and S.P. Mazzotti. 2005. Subduction zonne backarcs, mobile belts, and orogenic heat. *GSA Today* **15**:4–10.

Ivins, E.R., and C.G. Sammis. 1996. Transient creep of a composite lower crust, 1. Constitutive theory. *J. Geophys. Res.* **101**:B12, 27,981–28,004.

Jackson, J. 2002. Strength of the continental lithosphere: Time to abandon the jelly sandwich? *GSA Today* **12**:4–10.

Jade, S., M. Mukul, I.A. Parvez et al. 2002. Estimates of coseismic displacement and post-seismic deformation using Global Positioning System geodesy for the Bhuj earthquake of 26 January 2001. *Curr. Sci.* **82**:748–752.

Jaroslow, G.E., G. Hirth, and H.J.B. Dick. 1996. Abyssal peridotite mylonites: Implications for grain-size sensitive flow and strain localization in the oceanic lithosphere. *Tectonophysics* **256**:17–37.

Jarrard, R.D. 1986. Relations among subduction parameters. *Rev. Geophys.* **24**: 217–284.

Johnson, K.M., and P. Segall. 2004. Viscoelastic earthquake cycle models with deep stress-driven creep along the San Andreas fault system. *J. Geophys. Res.* **109**:B10403, doi:10.1029/2004JB003096.

Jónsson, S., P. Segall, R. Pedersen, and G. Björnsson. 2003. Post-earthquake ground movements correlated to pore-pressure transients. *Nature* **42**:179–183.

Kanamori, H., and T.H. Heaton. 2000. Microscopic physics of earthquakes. In: GeoComplexity and the Physics of Earthquakes, Geophys. Monogr. Ser. 120, pp. 147–163. Washington, D.C.: Am. Geophys. Union.

Karato, S., M.R. Riedel, and D.A. Yuen. 2001. Rheological structure and deformation of subducted slabs in the mantle transition zone: Implications for mantle circulation and deep earthquakes. *Phys. Earth & Planet. Inter.* **127**:83–108.

Kaufmann, G., and F. Amelung. 2000. Reservoir-induced deformation and continental rheology in the vicinity of Lake Mead, Nevada. *J. Geophys. Res.* **105**: 16,341–16,358.

Kenis, I., J.L. Urai, W. van der Zee, C. Hilgers, and M. Sintubin. 2005. Rheology of fine-grained siliciclastic rocks in the middle crust: Evidence from a combined structural and numerical analysis. *Earth Planet. Sci. Lett.* **233**:351–360.

Kenner, S., and P. Segall. 2003. Lower crustal structure in northern California: Implications from strain-rate variations following the 1906 San Francisco earthquake. *J. Geophys. Res.* **108**:doi: 10.1029/2001JB000189.

Kirby, S.H., W.B. Durham, and L.A. Stern. 1991. Mantle phase changes and deep-earthquake faulting in subducting lithosphere. *Science* **252**:216–225.

Klaper, E.M. 1990. Reaction-enhanced formation of eclogite-facies shear zones in granulite-facies anorthosites. In: Deformation Mechanisms, Rheology, and Tectonics, ed. R.J. Knipe and E.H. Rutter, Spec. Publ. 54, pp. 167–173. London: Geol. Soc.

Kohlstedt, D.L., B. Evans, and S.J. Mackwell. 1995. Strength of the lithosphere: Constraints imposed by laboratory experiments. *J. Geophys. Res.* **100**:17,587–17,602.

Knipe, R.J. 1989. Deformation mechanisms: Recognition from natural tectonites. *J. Struct. Geol.* **11**:127–146.

Küster, M., and B. Stöckhert. 1999. High differential stress and sublithostatic pore fluid pressure in the ductile regime: Microstructural evidence for short-term post-seismic creep in the Sesia Zone, Western Alps. *Tectonophysics* **303**:263–277.

Li, V.C., and J.R. Rice. 1987. Crustal deformation in Great California earthquake cycles. *J. Geophys. Res.* **92**:B11, 11,533–11,551.

Lin, S., D. Jiang, and P.F. Williams. 1998. Transpression (or transtension) zones of triclinic symmetry: Natural example and theoretical modelling. In: Continental Transpressional and Transtensional Tectonics, ed. J.F. Dewey, R.E. Holdsworth, and R.A. Strachan, Spec. Publ. 135, pp. 41–57. London: Geol. Soc.

Lister, G.S., M.A. Etheridge, and P.A. Symonds. 1991. Detachment models for the formation of passive continental margins. *Tectonics* **10**:1038–1064.

Lynch, J.C., R. Bürgmann, M.A. Richards, and R.M. Ferencz. 2003. When faults communicate: Viscoelastic coupling and earthquake clustering in a simple two-fault strike-slip system. *Geophys. Res. Lett.* **30**:doi:10.1029/2002-GL016765.

Maerklin, N., P.A. Bedrosian, C. Haberland et al. 2005. Characterizing a large shear zone with seismic and magnetotelluric methods: The case of the Dead Sea Transform. *Geophys. Res. Lett.* **32**:L15303, doi: 10.1029/2005GL022724.

Malservisi, R., C. Gans, and K.P. Furlong. 2002. Numerical modeling of creeping faults and implications for the Hayward fault, California. *Tectonophysics* **361**:121–137.

Mavko, G.M. 1981. Mechanics of motion on major faults. *Ann. Rev. Earth & Planet. Sci.* **9**:81–111.

Meissner, R., and J. Strehlau. 1982. Limits of stresses in continental crusts and their relation to the depth frequency distribution of shallow earthquakes. *Tectonics* **1**:73–89.

Miller, S.A. 2002. Properties of large ruptures and the dynamical influence of fluids on earthquakes and faulting. *J. Geophys. Res.* **107**:B9, doi: 10.1029/2000JB000032.

Miller, S.A., W. van der Zee, D.L. Olgaard, and J.A.D. Connolly. 2003. A fluid-pressure feedback model of dehydration reactions: Experiments, modelling, and application to subduction zones. *Tectonophysics* **370**:241–251.

Molnar, P. 1992. Brace-Goetze strength profiles, the partitioning of strike-slip and thrust faulting at zones of oblique convergence, and the stress–heat flow paradox of the San Andreas fault. In: Fault Mechanics and Transport Properties of Rocks: A Festschrift in Honor of W.F. Brace, ed. B. Evans, and T.F. Wong, Intl. Geophys. Ser. 51, pp. 435–460. London: Academic Press.

Montesi, L.G.J. 2004. Postseismic deformation and the strength of ductile shear zones. *Earth Planet & Space* **56**:1135–1142.

Montesi, L.G.J., and G. Hirth. 2003. Grain size evolution and the rheology of ductile shear zones: From laboratory experiments to postseismic creep. *Earth Planet. Sci. Lett.* **211**:97–110.

Moore, D., D.A. Lockner, M. Shengli, R. Summers, and J. Byerlee. 1997. Strengths of serpentinite gouges at elevated temperatures. *J. Geophys. Res.* **102**:14,787–14,801.

Mulch, A., and M.A. Cosca. 2004. Recrystallization or cooling ages: *In situ* UV laser ^{40}Ar/^{39}Ar geochronology of muscovite in mylonitic rocks. *J. Geol. Soc. Lond.* **161**:573–582.

Mulch, A., M.A. Cosca, and M.R. Handy. 2002. *In situ* UV laser ^{40}Ar/^{39}Ar geochronology of a micaceous mylonite: An example of defect-enhanced argon loss. *Contrib. Mineral. & Petrol.* **142**:738–752.

Müller, W., D. Aerden, and A.N. Halliday. 2000. Isotopic dating of strain fringe increments: Duration and rates of deformation in shear zones. *Science* **288**:2195–2198.

Nishimura, T., and W. Thatcher. 2003. Rheology of the lithosphere inferred from postseismic uplift following the 1959 Hebgen Lake earthquake. *J. Geophys. Res.* **108**:B8, doi:10.1029/2002JB002191.

Otsuki, K., N. Monzawa, and T. Nagase. 2003. Fluidization and melting of fault gouge during seismic slip: Identification in the Nojima fault zone and implications for focal earthquake mechanisms. *J. Geophys. Res.* **108**:B4, 2192 doi:10.1029/2001JBB001711.

Palm, S. 1999. Verformungsstrukturen und gesamtgesteinsgeochemische Alteration nahe dem spröd-viskosen Übergang an der Pogallo-Störungszone (Norditalien), Ph.D. Diss., Justus-Liebig-Univ. Giessen, Germany.

Paterson, M.S. 1995. A granular flow approach to superplasticity. In: Plastic Deformation of Ceramics, ed. R.C. Bradt, pp. 279–283. New York: Plenum Press.

Paterson, M.S. 2001. Relating experimental and geological rheology. *Intl. J. Earth Sci.* **90**:149–156.

Peltzer, G., P. Rosen, F. Rogez, and K. Hudnut. 1996. Postseismic rebound in fault step-overs caused by pore fluid flow. *Science* **273**:1202–1204.

Platt, J.P. 1984. Secondary cleavages in ductile shear zones. *J. Struct. Geol.* **6**:439–442.

Platt, J.P., and R.L.M. Vissers. 1980. Extensional structures in anisotropic rocks. *J. Struct. Geol.* **2**:397–410.

Pollitz, F.F., R. Bürgmann, and P. Segall. 1998. Joint estimation of afterslip rate and postseismic relaxation following the 1989 Loma Prieta earthquake. *J. Geophys. Res.* **103**:26,975–26,992.

Pollitz, F.F., G. Peltzer, and R. Bürgmann. 2000. Mobility of continental mantle: Evidence from postseismic geodetic observations following the 1992 Landers earthquake. *J. Geophys. Res.* **105**:8035–8054.

Pollitz, F.F., C. Wicks, and W. Thatcher. 2001. Mantle flow beneath a continental strike-slip fault: Postseismic deformation after the 1999 Hector Mine earthquake. *Science* **293**:1814–1818.

Prior, D.J., R.J. Knipe, and M.R. Handy. 1990. Estimates of the Rates of Microstructural Change in Mylonites, Spec. Publ. 54, pp. 309–320. London: Geol. Soc.

Ramsay, J.G., and R.H. Graham. 1970. Strain variation in shear belts. *Canad. J. Earth Sci.* **7**:786–813.

Ranalli, G., and D.C. Murphy. 1987. Rheological stratification of the lithosphere. *Tectonophysics* **132**:281–296.

Reddy, S.M., and G.J. Potts. 1999. Constraining absolute deformation ages: The relationship between deformation mechanisms and isotope systematics. *J. Struct. Geol.* **21**:1255–1265.

Rolandone, F., R. Bürgmann, and R.M. Nadeau. 2004. The evolution of the seismic–aseismic transition during the earthquake cycle: Constraints from the time-dependent depth distribution of aftershocks. *Geophys. Res. Lett.* **31**:L23610, doi:10.1029/2004GL21379.

Rudnicki, J.W., and J.R. Rice. 1975. Conditions for the localization of deformation in pressure-sensitive dilatant materials, *J. Mech. Phys. Solids* **23**:371–394.

Rutter, E.H., and K.H. Brodie. 2004. Experimental grain size-sensitive flow of hot-pressed Brazilian quartz aggregates. *J. Struct. Geol.* **26**:2011–2023.

Savage, J.C. 1990. Equivalent strike-slip earthquake cycles in half-space and lithosphere–asthenosphere earth models. *J. Geophys. Res.* **95**:4873–4879.

Savage, J.C., and R.O. Burford. 1970. Accumulation of tectonic strain in California. *Bull. Seismol. Soc. Am.* **60**:1877–1896.

Schaff, D.P., G.H.R. Bokelmann, G.C. Beroza, F. Waldhauser, and W.L. Ellsworth. 2002. High resolution image of Calaveras fault seismicity. *J. Geophys. Res.* **107**:doi:10.1029/2001JB000633.

Schmid, S.M., and M.R. Handy. 1991. Towards a genetic classification of fault rocks: Geological usage and tectonophysical implications. In: Controversies in Modern Geology, ed. K.J. Hsü, J. Mackenzie, and D. Müller, pp. 339–361. London: Academic Press.

Schmidt, D.A. 2002. The kinematics of faults in the San Francisco Bay area inferred from geodetic and seismic data. Ph.D. thesis. Berkeley: Univ. California, Berkeley.

Scholz, C. 1992. Paradigms or small change in earthquake mechanics. In: Fault Mechanics and Transport Properties of Rocks: A Festschrift in Honor of W.F. Brace, ed. B. Evans, and T.F. Wong, Intl. Geophys. Ser. 51, pp. 435–460. London: Academic Press.

Scholz, C.H. 1998. Earthquakes and friction laws. *Nature* **391**:37–42.

Schreurs, G. 1994. Experiments on strike-slip faulting and block rotation. *Geology* **22**:567–570.

Schwarz, S., and B. Stöckhert. 1996. Pressure solution in siliciclastic HP-LT metamorphic rocks: Constraints on the state of stress in deep levels of accretionary complexes. *Tectonophysics* **255**:203–209.

Secor, Jr., D.T. 1965. Role of fluid pressure in jointing. *Am. J. Sci.* **263**:633–646.

Segall, P. 2002. Integrating geologic and geodetic estimates of slip rate on the San Andreas fault system. *Intl. Geol. Rev.* **44**:62–82.

Sibson, R.H., and J.V. Rowland. 2003. Stress, fluid pressure, and structural per-meability in seismogenic crust, North Island, New Zealand. *Geophys. J. Intl.* **154**:584–594.

Sleep, N.H. 1995. Ductile creep, compaction, and rate- and state-dependent friction within major fault zones. *J. Geophys. Res.* **100**:13,065–13,080.

Stein, R.S. 1999. The role of stress transfer in earthquake occurrence. *Nature* **402**:605–609.

Stipp, M., H. Stünitz, R. Heilbronner, and S.M. Schmid. 2002. Dynamic recrystallization of quartz: Correlation between natural and experimental conditions. In: Deformation Mechanisms, Rheology, and Tectonics: Current Status and Future Perspectives, ed. S. De Meer, M.R. Drury, J.H.P. De Bresser, and G.M. Pennock, Spec. Publ. 200, pp. 171–190. Lond.: Geol. Soc.

Stipp, M., and J. Tullis. 2003. The recrystallized grain size piezometer for quartz. *Geophys. Res. Lett.* **30**:2008, doi:10.1029/2003GL018444.

Stone, D.S., T. Plookphol, and R.F. Cooper. 2004. Similarity and scaling in creep and load relaxation of single-crystal halite (NaCl). *J. Geophys. Res.* **109**:B12201, doi:10.1029/2004JB003064.

Stöckhert, B., M.R. Brix, R. Kleinschrodt, A.J. Hurford, and R. Wirth. 1999. Thermochronometry and quartz microstructures – A comparison with experimental flow laws and predictions on the brittle-plastic transition. *J. Struct. Geol.* **21**:351–369.

Stünitz, H., and J.D. FitzGerald. 1993. Deformation of granitoids at low metamorphic grade. II: Granular flow in albite-rich mylonites. *Tectonophysics* **221**:299–324.

Tchalenko, J.S. 1970. Similarities between shear zones of different magnitudes. *Geol. Soc. Am. Bull.* **81**:1625–1640.

Teyssier, C., B. Tikoff, and J. Weber. 2002. Attachment between brittle and ductile crust at wrenching plate boundaries. Stephan Mueller Spec. Publ. Ser. 1, pp. 119–144. European Geosciences Union (EGU).

Thatcher, W. 1983. Nonlinear strain buildup and the earthquake cycle on the San Andreas fault. *J. Geophys. Res.* **88**:5893–5902.

Trepmann, C., and B. Stöckhert. 2003. Quartz microstructures developed during non-steady state plastic flow at rapidly decaying stress and strain rate. *J. Struct. Geol.* **25**:2035–2051.

Trompert, R., and U. Hansen. 1998. Mantle convection simulations with rheologies that generate plate-like behaviour. *Nature* **395**:686–689.

Tse, S.T., and J.R. Rice. 1986. Crustal earthquake instability in relation to the depth variation of frictional slip properties. *J. Geophys. Res.* **91**:B9, 9452–9472.

Tullis, T.E., F.G. Horowitz, and J. Tullis. 1991. Flow laws of polyphase aggregates from end-member flow laws. *J. Geophys. Res.* **96**:B5, 8081–8096.

Vauchez, A., and A. Tommasi. 2003. Wrench faults down to the asthenosphere: geological and geophysical evidence and thermo-mechanical effects. In: Intraplate Strike-Slip Deformation Belts, ed., F. Storti, R.E. Holdsworth, and F. Salvani, Spec. Publ. 210, pp. 15–34. London: Geol. Soc.

Villa, I.M. 1998. Isotopic closure. *Terra Nova* **10**:42–47.

Vissers, R.L.M., M.R. Drury, E.H. Hoogerduijn Strating, and D. Van der Wal. 1995. Mantle shear zones and their effect on lithosphere strength during continental breakup. *Tectonophysics* **249**:155–171.

White, S.H., M.R. Drury, S.E. Ion, and F.J. Humphreys. 1985. Large strain deformation studies using polycrystalline magnesium as a rock analogue. Part I: Grain-size paleopiezometry in mylonite zones. *Phys. Earth & Planet. Inter.* **40**:201–207.

Wittlinger, G., P. Tapponnier, G. Poupinet et al. 1996. Tomographic evidence for localized lithospheric shearing along the Altyn Tagh fault. *Science* **282**:74–76.

Zingg, A., M.R. Handy, J.C. Hunziker, and S.M. Schmid. 1990. Tectonometamorphic history of the Ivrea Zone and its relation to the crustal evolution of the Southern Alps. *Tectonophysics* **182**:169–192.

Zoback, M.D., and H.-P. Harjes. 1997. Injection-induced earthquakes and crustal stress at 9 km depth at the KTB deep drilling site. Germany. *J. Geophys. Res.* **102**:B8, 18,477–18,491.

Zoback, M.D., and J. Townend. 2001. Implication of hydrostatic pore pressures and high crustal strength for the deformation of intraplate lithosphere. *Tectonophysics* **336**:19–30.